

Australian Rainfall & Runoff

Revision Projects

PROJECT 18

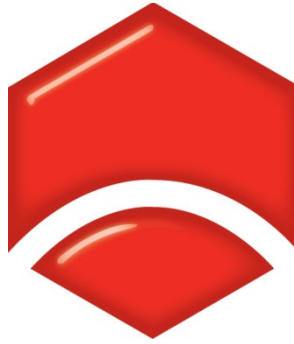
Coincidence of Fluvial Flooding
Events and Coastal Water
Levels in Estuarine Areas

STAGE 3 REPORT

P18/S3/011

DECEMBER 2014





**ENGINEERS
AUSTRALIA**
Water Engineering

Engineers Australia
Engineering House
11 National Circuit
Barton ACT 2600


Tel: (02) 6270 6528
Fax: (02) 6273 2358
Email: arr_admin@arr.org.au
Web: www.arr.org.au

AUSTRALIAN RAINFALL AND RUNOFF

**REVISION PROJECT 18: COINCIDENCE OF FLUVIAL FLOODING EVENTS AND
COASTAL WATER LEVELS IN ESTUARINE AREAS**

STAGE 3 REPORT

DECEMBER, 2014

Project Revision project 18: Coincidence of Fluvial Flooding Events and Coastal Water Levels in Estuarine Areas	AR&R Report Number P18/S3/011
Date 1 December 2014	ISBN 978-085825-9935
Contractor The University of Adelaide	Contractor Reference Number A124141
Authors Feifei Zheng Seth Westra Michael Leonard	Verified by 

ACKNOWLEDGEMENTS

This project was made possible by funding from the Federal Government through the Department of Climate Change. This report and the associated project are the result of a significant amount of in kind hours provided by Engineers Australia Members.



ENGINEERS
AUSTRALIA
Water Engineering



THE UNIVERSITY
of ADELAIDE

Draft

Discussion

FOREWORD

AR&R Revision Process

Since its first publication in 1958, Australian Rainfall and Runoff (ARR) has remained one of the most influential and widely used guidelines published by Engineers Australia (EA). The current edition, published in 1987, retained the same level of national and international acclaim as its predecessors.

With nationwide applicability, balancing the varied climates of Australia, the information and the approaches presented in Australian Rainfall and Runoff are essential for policy decisions and projects involving:

- infrastructure such as roads, rail, airports, bridges, dams, stormwater and sewer systems;
- town planning;
- mining;
- developing flood management plans for urban and rural communities;
- flood warnings and flood emergency management;
- operation of regulated river systems; and
- prediction of extreme flood levels.

However, many of the practices recommended in the 1987 edition of AR&R now are becoming outdated, and no longer represent the accepted views of professionals, both in terms of technique and approach to water management. This fact, coupled with greater understanding of climate and climatic influences makes the securing of current and complete rainfall and streamflow data and expansion of focus from flood events to the full spectrum of flows and rainfall events, crucial to maintaining an adequate knowledge of the processes that govern Australian rainfall and streamflow in the broadest sense, allowing better management, policy and planning decisions to be made.

One of the major responsibilities of the National Committee on Water Engineering of Engineers Australia is the periodic revision of ARR. A recent and significant development has been that the revision of ARR has been identified as a priority in the Council of Australian Governments endorsed National Adaptation Framework for Climate Change.

The update will be completed in three stages. Twenty one revision projects have been identified and will be undertaken with the aim of filling knowledge gaps. Of these 21 projects, ten projects commenced in Stage 1 and an additional 9 projects commenced in Stage 2. The remaining two projects will commence in Stage 3. The outcomes of the projects will assist the ARR Editorial Team with the compiling and writing of chapters in the revised ARR.

Steering and Technical Committees have been established to assist the ARR Editorial Team in guiding the projects to achieve desired outcomes. Funding for Stages 1 and 2 of the ARR revision projects has been provided by the Federal Department of Climate Change and Energy Efficiency. Funding for Stages 2 and 3 of Project 1 (Development of Intensity-Frequency-Duration information across Australia) has been provided by the Bureau of Meteorology.

Project 18: Interaction of coastal processes and severe weather events

Flooding in the downstream regions of many coastal catchments is the result of the interaction between runoff generated by a weather event that elevates sea levels and/or estuary water levels. Historically assumptions have been made regarding either the independence of these events or the timing of rainfall or flood peaks and peak ocean and/or estuarine conditions, for example peak runoff and peak ocean or estuary levels coinciding. Assuming that the weather events that generated elevated ocean or estuary conditions and significant catchment runoff are independent can underestimate flood levels in coastal areas. Conversely an assumption that the flood peak coincides with the peak elevated ocean or estuary conditions can overestimate flood levels in coastal areas. In order to better understand flooding in coastal areas it is necessary to have an understanding of the role that severe weather conditions that create elevated ocean or estuary conditions have in generating catchment runoff that floods coastal areas.

The importance of this understanding will increase in time as existing coastal communities are threatened increasingly by sea level rise as a result of climate change.



Mark Babister

Chair Technical Committee for
ARR Research Projects



Assoc Prof James Ball

ARR Editor

AR&R REVISION PROJECTS

The 21 AR&R revision projects are listed below:

ARR Project No.	Project Title	Starting Stage
1	Development of intensity-frequency-duration information across Australia	1
2	Spatial patterns of rainfall	2
3	Temporal pattern of rainfall	2
4	Continuous rainfall sequences at a point	1
5	Regional flood methods	1
6	Loss models for catchment simulation	2
7	Baseflow for catchment simulation	1
8	Use of continuous simulation for design flow determination	2
9	Urban drainage system hydraulics	1
10	Appropriate safety criteria for people	1
11	Blockage of hydraulic structures	1
12	Selection of an approach	2
13	Rational Method developments	1
14	Large to extreme floods in urban areas	3
15	Two-dimensional (2D) modelling in urban areas.	1
16	Storm patterns for use in design events	2
17	Channel loss models	2
18	Interaction of coastal processes and severe weather events	1
19	Selection of climate change boundary conditions	3
20	Risk assessment and design life	2
21	IT Delivery and Communication Strategies	2

AR&R Technical Committee:

Chair: Mark Babister, WMAwater

Members: Associate Professor James Ball, Editor AR&R, UTS

Professor George Kuczera, University of Newcastle

Professor Martin Lambert, University of Adelaide

Dr Rory Nathan, SKM

Dr Bill Weeks

Associate Professor Ashish Sharma, UNSW

Dr Bryson Bates, CSIRO

Steve Finlay, Engineers Australia

Related Appointments:

ARR Project Engineer:

Monique Retallick, WMAwater

ARR Admin Support:

Isabelle Testoni, WMAwater

PROJECT TEAM AND ACKNOWLEDGEMENTS

The research for this project was conducted by Drs Feifei Zheng, Seth Westra and Michael Leonard.

Acknowledgements: Discussions with a number of people assisted in the compilation of this report. Specifically, I would like to acknowledge Dr John Hunter who provided valuable feedback on the Australian storm surge record and the meteorological drivers of surge; Mr Kirby Campbell-Wood for assisting with data compilation and testing; Drs Peter Hawke (HR Wallingford) and Cecilia Svensson (UK Centre of Ecology and Hydrology) for providing information on the methodology currently used in the UK; Mr Paul Davill (National Tidal Centre) for providing input on the storm tide data used in this project; and Ms Lisa Colby and Mr Tim Pearce (both from Water Corporation) and Mr Mark Babister, Mr Ivan Varga and Ms Erin Askew (from WMA Water) for contributing data and modelling for the case studies in this report. Finally, we would like to acknowledge the contribution of A/Prof Scott Sisson (Department of Mathematics and Statistics, University of New South Wales) who provided significant statistical support in the development of the extreme value models used in this project.

The tidal data was collated by Mr Alex Osti from EngTest at Adelaide University, with further details on the dataset provided in a separate report (EngTest, 2010). This involved obtaining licences to use data from a range of harbour and port authorities, which are listed as follows:

- Sydney Ports Corporation;
- Maritime Authority of NSW;
- Newcastle Port Corporation;
- Port Kembla Port Corporation;
- Department of Planning and Infrastructure, Northern Territory;
- Maritime Safety Queensland;
- Flinders Ports;
- TasPorts;
- Victorian Regional Channels Authority;
- Port of Melbourne Corporation;
- Bureau of Meteorology;
- Port of Portland;
- Patrick Ports;
- Albany Port Authority;
- Broome Port Authority;
- Bunbury Port Authority;

- Coastal Data Centre,
- WA Department of Transport;
- Esperance Ports Sea and Land;
- Fremantle Ports;
- Geraldton Port Authority;
- Dampier Port Authority; and
- Port Headland Port Authority.

This report was independently reviewed by:

Draft for discussion

EXECUTIVE SUMMARY

Floods in coastal catchments can be caused by runoff generated by an extreme rainfall event, elevated sea levels due to an extreme storm tide event, or a combination of both processes occurring simultaneously or in close succession. Statistical dependence between extreme rainfall and extreme storm surge is common as both variables are often driven by the same meteorological processes. This can lead to higher flood levels compared to the case when these processes are independent.

This report presents the outcomes of an investigation into the statistical dependence of these processes along the Australian coastline, and describes how this information could be used to estimate flood risk. The analysis was supported by the most extensive dataset of observational records currently available, comprising a total of 64 tide gauges, 7,684 daily rainfall stations, and 70 sub-daily rainfall stations. The specific outcomes are as follows:

- (1) The majority of the Australian coastline exhibits weak yet statistically significant dependence. The relationship between extreme rainfall and storm surge was found to be 'asymptotically dependent', which means that the dependence either remains constant or strengthens as the rainfall and storm surge become more extreme.
- (2) The dependence strength varies as a function of the spatial distance between the rainfall and tide gauges, with the rainfall gauges that are closest to the tide gauge exhibiting the strongest dependence. In addition, the rainfall gauges that are located in the vicinity of the coastline show overall stronger dependence than those located further inland.
- (3) The duration of the storm burst is an important factor that affects dependence strength. For durations from 15 minutes to 24 hours, the dependence mostly becomes stronger with increasing duration. For longer storm burst durations, some zones exhibit stronger dependence, while other zones exhibit approximately constant or slightly weaker dependence relative to 24 hour durations.
- (4) The influence of the lag (time delay) between the extreme rainfall and extreme storm surge has also been investigated. The results show that extreme rainfall is more likely to occur after the extreme storm surge, although dependence at lag zero is also statistically significant. The lagged timing of the strongest dependence varies with location and storm burst duration.
- (5) A dependence map has been developed for the Australian coastline (Figure E1). The dependence between extreme rainfall and storm surge is represented by the parameter α for storm burst durations shorter than 12 hours ($T < 12$ hours), between 12 hours and 48 hours ($12 \text{ hours} \leq T \leq 48 \text{ hours}$) and greater than 48 hours ($48 \text{ hours} < T \leq 168 \text{ hours}$). The range of α is $[0,1]$, with a larger value of α indicating weaker dependence ($\alpha = 0$ and $\alpha = 1$ represent complete dependence and independence respectively).

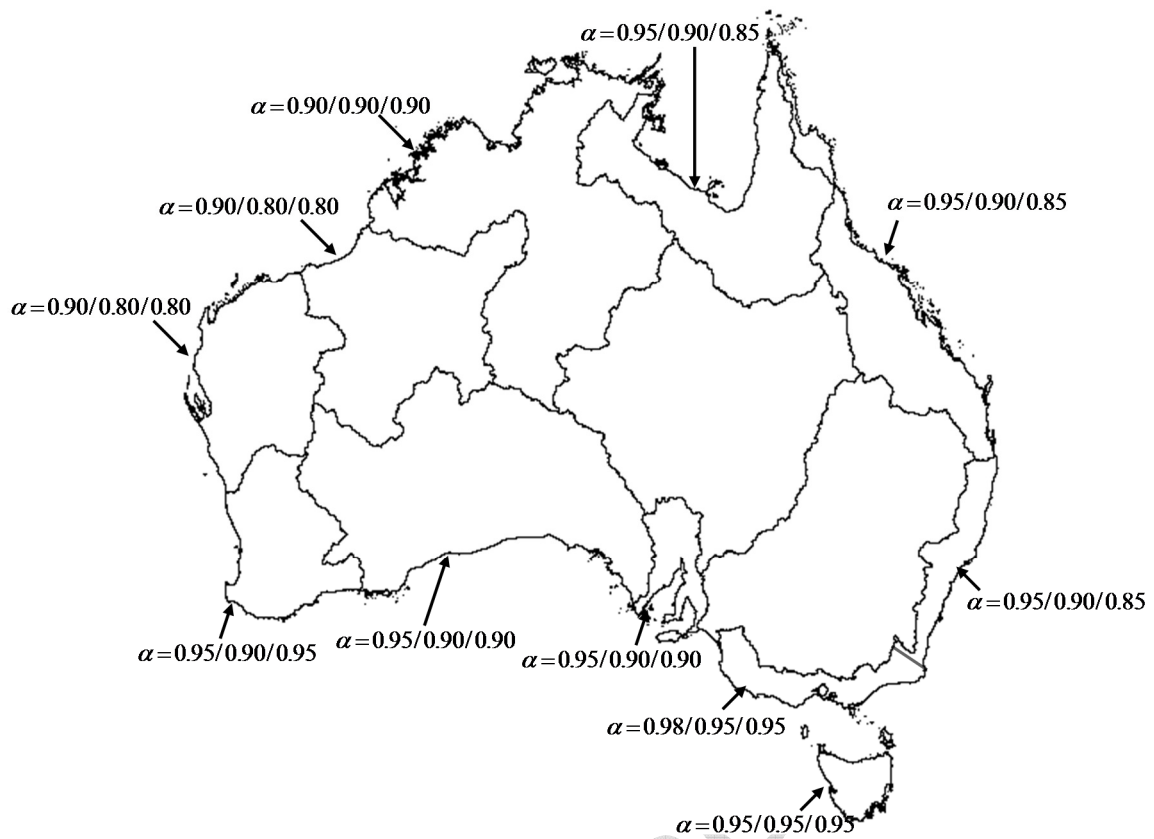


Figure E1. Map of dependence values for the basins along the Australian coastline. The three values of the dependence parameter (α) in each region represent the dependence strength for storm burst durations shorter than 12 hours, between 12 and 48 hours, and between 48 and 168 hours, respectively. Values closer to 1 represent weaker dependence, whereas values closer to 0 represent stronger dependence.

Based on this analysis, a design variable method is described to account for the dependence between extreme rainfall and storm surge/tide, and is recommended for inclusion into Australian Rainfall Runoff (ARR) as an approach for estimating coastal flood risk. The design variable method has four steps:

- i. a pre-screening analysis that estimates the difference in flood levels between the complete independence and complete dependence cases, to identify situations where the implications of dependence are sufficiently significant to warrant further detailed modelling;
- ii. the selection of the dependence parameter based on the catchment location and the storm burst duration;
- iii. the estimation of a table of flood levels corresponding to different combinations of extreme rainfall and storm tide exceedance probabilities, using hydrologic/hydraulic models; and
- iv. estimation of flood levels based on the dependence parameter obtained in step (ii) and the flood level table obtained in step (iii).

The method assumes static tailwater levels and requires simulation of extreme rainfall and storm

tide events, and is not designed to account for dynamical features related to tides and surges. The method has been tested for floods ranging from the 50 % annual exceedance probability (AEP) event to the 1 % AEP event. The implementation described in this report does not estimate of uncertainty bounds and nor does it account for the implications of anthropogenic climate change, although it is likely that the method can be adjusted to take both issues into account.

The design variable method described here has been derived as an internally consistent and theoretically sound approach for accounting for dependence between extreme rainfall and storm surge/tide along the Australian coastline, and is likely to be applicable for a wide range of conditions. However it is noted that alternative methods, such as those based on time-stepping continuous simulation models, may also be appropriate in certain circumstances. Therefore in addition to recommending the design variable method, it is also recommended that the ARR guidance not preclude the use of alternative approaches where they can be theoretically justified.

Draft for discussion

TABLE OF CONTENTS

1.	Introduction.....	12
1.1.	Objectives.....	12
1.2.	Outcomes	13
1.3.	Report structure.....	13
2.	A review of joint dependence modelling.....	14
2.1.	The quantification of the dependence strength	14
2.2.	The incorporation of the dependence for flood risk analysis.....	15
3.	Data.....	17
3.1.	Tidal records.....	17
3.2.	Daily Rainfall Records	23
3.3.	Sub-daily Rainfall Records.....	24
3.4.	The data paired for the dependence analysis	24
4.	Assessment of the asymptotic properties of the joint dependence.....	27
5.	Statistical models used for dependence analysis.....	30
5.1.	Representation of bivariate extremes.....	30
5.2.	Bivariate extreme value theory	31
5.3.	Selection of bivariate extreme value model.....	33
6.	Results of dependence study	35
6.1.	Interpretation of the dependence parameter α	35
6.2.	Spatial variation of dependence.....	36
6.3.	The impact of storm burst duration on dependence.....	38
6.4.	The impact of lags on dependence	39
6.5.	Dependence map of the Australian coastline	41
7.	The method used for incorporating dependence for flood risk analysis.....	44
8.	Recommended guidance to be included in Australian Rainfall and Runoff	46
9.	Case studies.....	51
9.1.	Case Study 1 – The Perth drainage system.....	51
9.2.	Case Study 2- Nambucca River catchment	54

10.	Summary and Conclusions	61
10.1.	Development of a map representing dependence strength.....	61
10.2.	A method to translate dependence to estimates of flood risk.....	62
10.3.	Exclusions and further research.....	63
11.	References	66
	Appendix A – Information on the sub-daily rainfall gauges	68
	Appendix B – Procedures for obtaining the dependence parameter	69
	Appendix C – Selecting the statistical model	72
	Appendix D –The detailed results for each tide gauge	78

Draft for discussion

1. Introduction

Floods in coastal catchments can be caused by runoff generated by an extreme rainfall event, elevated sea levels due to an extreme storm surge event, or a combination of both processes occurring simultaneously or in close succession. Statistical dependence between extreme rainfall and extreme storm surge is likely as both variables can be driven by common meteorological forcings. Tropical cyclones, for example, may produce strong onshore winds and an inverse barometric effect, leading to an extreme storm surge, while simultaneously generating large quantities of rainfall on the adjacent coastal catchments.

The recent Intergovernmental Panel on Climate Change (IPCC) Special Report on Extremes (SREX 2012) identified a broad class of natural hazards that are caused by a combination of physical processes and referred to these as 'compound events' (see also Leonard *et al.*, 2013). In the IPCC's report, the importance of understanding the interaction between different physical forcing factors has been highlighted in order to evaluate the risk of natural hazards. In the context of flood risk analysis along the Australian coastline, it is critical to understand the interaction (dependence) between extreme rainfall and extreme storm surge in order to correctly estimate the coastal flood risk.

1.1. Objectives

The report describes the outcome of Stage 3 of Project 18 of the Australian Rainfall and Runoff Revision. The overall aim of this project is to investigate the spatial and temporal variations of the dependence between extreme rainfall and extreme storm surge along the Australian coastline, and incorporate this dependence into flood risk analysis. This research project follows on from the Stage 2 of Project 18 of Australian Rainfall and Runoff Revision (Westra, 2012), with specific objectives given as follows.

1. A detailed investigation of the strength of dependence between extreme rainfall and storm surge at all locations identified in Westra (2012) for which adequate storm surge data is available.
2. Development of a map to show the spatial variation of the dependence along the Australian coastline.
3. A detailed investigation of the influence of temporal variability (storm burst duration) on the dependence along the Australian coastline.
4. Development of a method to determine where dependence can be ignored or treated simply.
5. Development of a method to incorporate the dependence between extreme rainfall and surge within the hydrologic/hydraulic model framework currently used in practice.
6. Testing of the method for a number of case study locations around the Australian coastline.

1.2. Outcomes

The dependence between extreme rainfall and extreme storm surge has been quantified along the Australian coastline, and a method has been developed to account for such dependence into flood risk analysis. The main outcomes of this project are given as follows.

1. A dependence map for the Australian coastline that can be used as the basis for incorporating dependence into flood risk analysis.
2. A proposed four-step method for translating this dependence into estimates of flood risk.
3. An R package that is used to transform the dependence into flood levels
4. Four internationally peer-reviewed journal papers and one conference paper:
 - Zheng, F., S. Westra, and S. A. Sisson (2013a), *Quantifying the dependence between extreme rainfall and storm surge in the coastal zone*, Journal of Hydrology, 505(0), 172-187.
 - Zheng, F., Westra S. Sisson S. and Leonard M. (2014). *Modelling the dependence between extreme rainfall and storm surge to estimate coastal flood risk*, Water Resources Research, 50, 2050-2071.
 - Zheng, F. Leonard M. and Westra S. *An efficient bivariate integration method for estimating flood risk*, Journal of Hydroinformatics, submitted.
 - Zheng, F. Leonard M. and Westra S. *Application of the design variable method to estimate coastal flood risk*, Journal of Flood Risk Management, submitted.
 - Zheng, F., Westra S. Sisson S. and Leonard M. (2013e). *Flood risk estimation in Australia's coastal zone: modelling the dependence between extreme rainfall and storm surge*, 35th Hydrology and Water Resources Symposium, 24 – 27 February 2014, Perth, Australia,
5. This report, which describes the outcomes of the overall research project.

1.3. Report structure

The structure of the report is organized as follows. Chapter 2 briefly describes previous work on joint dependence analysis, followed by a description of the daily rainfall, sub-daily rainfall and storm tide records used for the analysis in Chapter 3. Chapters 4 and 5 present preliminary analyses of the data and statistical models used for dependence analysis. The results of the dependence study and the method are respectively described in Chapters 6 and Chapter 7. Chapter 8 shows the recommended guidance based on the results of this research project. Finally Chapter 9 and 10 present case studies and conclusions of this work.

2. A review of joint dependence modelling

2.1. The quantification of the dependence strength

The presence of statistical dependence between extreme rainfall and storm surge has been recognized for a long time, and numerous attempts have been made to quantify its strength. Coles *et al.* (1999), for example, conducted an analysis between rainfall and surge events in southern England, and Svensson and Jones (2002) investigated the dependence between high sea surges, river flow and precipitation in eastern Britain. Both studies found statistically significant dependence between extreme rainfall and extreme storm surge.

Svensson and Jones (2004) explored the dependence between extreme rainfall and extreme surge in the south and west of Britain, showing that the strength of the dependence was governed by a range of factors, including meteorological conditions, orographic properties of the catchment (slope and orientation), and the lag between the two extreme events. In another study, Svensson and Jones (2006) found that the dependence between extreme rainfall and storm surge was statistically significant and needed to be taken into account for flood risk estimation, although spatial variability of the dependence strength was also observed. Svensson and Jones (2006) and Hawkes and Svensson (2006) provided dependence maps for England, Scotland and Wales and developed guidelines for when and how joint probability methods should be used. White (2009) investigated the dependence between river flow, tide and surge for Lewes, East Sussex, UK, a town which is prone to both tidal and fluvial flooding. A low but significant level of dependence between river flow and sea level was detected for this region, but a much higher level of dependence was observed between river flow and the storm surge residual.

More recently, Lian *et al.* (2013) quantified dependence between extreme rainfall and storm surge in a coastal city with a complex river network. The flood severity under the combined effect of rainfall over the catchment and the tide levels in the lower reaches was assessed in their study. Results show that the joint impact of these two processes has a significant influence on flood risk.

Statistical models play an important role in quantifying dependence between extremes. Although a number of statistical models have been available for modelling extremes, the threshold-excess and point process methods represent the most commonly studied types of multivariate extreme modelling approaches (Coles 2001). The advantages of these two methods include that (i) their fitting procedures do not require advanced computational techniques, and (ii) they possess a relatively simple and flexible structure. Details of the threshold-excess and point process models are given in Section 5 of this report.

2.2. The incorporation of the dependence for flood risk analysis

Having characterised the dependence between extreme rainfall and extreme storm surge at a given location, it is necessary to incorporate such a relationship into estimates of flood risk. This problem is more challenging than the situation where floods are caused by only a single physical process, because the return period of the forcing processes are no longer equivalent to the return period of the flood (Callaghan and Helman, 2008; Hawkes et al, 2002). To address this issue, Coles and Tawn (1994) proposed a method referred to as a 'structure function', for which the multiple extremes are translated into a single variable of interest. Details of the structure function method are given in Chapter 7.

Alternatively, multivariate processes can be reduced to a single variable of interest as discussed by Bortot *et al.*, 2000 (often referred to as the 'structure variable method'). Univariate extreme value theory is then used to estimate the return probabilities of the single variable. An advantage of the structure variable method is that it is conceptually straightforward. However, it can be computationally demanding in practice as it requires a continuous simulation approach. In order to obtain sequences of the design variable (e.g. annual maximum or peak over threshold water levels) this approach requires hydrologic/hydrodynamic models to be forced by long sequences of observed rainfall and storm tides as boundary conditions; in many cases long sequences of the forcing data would not be available, and the computational cost of such an analysis would likely be significant.

In the context of flood risk analysis along the Australian coastline, Haigh et al. (2013) conducted modelling to provide estimates of storm tide levels, and Hunter (2011) demonstrate the benefits of statistical models that can incorporate mean sea level into estimates of extremes, but these methods do not consider estuarine regions that are also affected by rainfall. There is currently limited information for estimating floods that account for the dependence between extreme rainfall and extreme storm surge, although the importance of accounting for such dependence has often been recognised. For example, the NSW Department of Environment, Climate Change and Water released guidelines on incorporating ocean boundary conditions into flood modelling (NSW DECCW, 2009). This guideline recommends using an 'envelope' approach to combine different upper and lower boundary conditions in terms of marginal annual exceedance probability (AEP) values. For example, the 1% AEP flood level is estimated by assuming 1% AEP rainfall over the catchment combined with 5% AEP tide level in the lower reach of the catchment. However, it is unknown whether such a scenario would actually represent or approximate the true joint dependence between these two variables, as the dependence strength would like vary as a function of factors like geographic location and the duration of the storm event, amongst other things.

There is therefore a need to quantify the joint dependence between extreme rainfall and extreme storm surge and translate it into methods of flood risk estimation. There are many factors that influence the role that dependence might play in any particular flood estimation study and the relevance of these factors needs to be considered by any proposed method. For example, as was shown by Westra (2012), the dependence varies as a function of spatial distances between tide gauges and rainfall gauges, different storm burst durations and timing of lags between extreme rainfall and storm surge.

This research project addresses the issues mentioned above. It is envisaged that, by better understanding the dependence between rainfall and storm surge processes in estuarine areas, this information will provide a necessary precursor to more accurate estimates of flood risk along the Australian coastline.

Draft for discussion

3. Data

This research investigates the presence of joint dependence between extreme rainfall and storm surge using the most extensive observational records of rainfall and storm surge events currently available. A brief description of the storm surge/tide records and the daily and sub-daily rainfall records used in this study is given below.

3.1. Tidal records

Two separate tidal datasets were made available for this study. The first dataset comprises 15 tide gauges with high-quality records for the period from 1991 to 2010, which was collected as part of the Australian Baseline Sea Level Monitoring Project (ABSLMP). The second dataset comprises 49 tide gauges with record lengths greater than 20 years. The locations of the tide gauges from both datasets are presented in Figure 3.1, with further details provided in Tables 3.1 and 3.2.

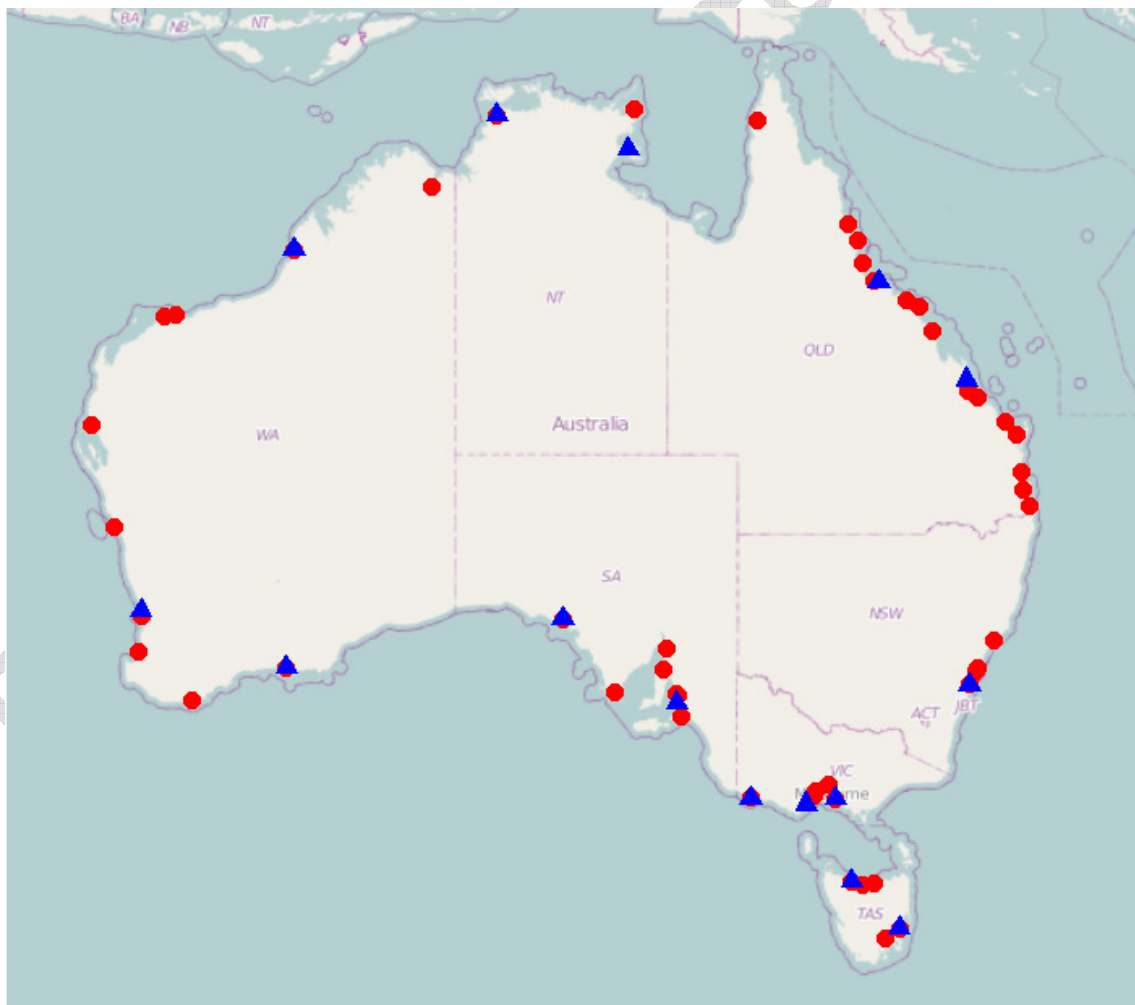


Figure 3.1: Location of tide gauge locations. The location of tide gauges from the Australian Baseline Sea Level Monitoring Project (ABSLMP) are presented as blue triangles, and the location of the remaining 49 tide gauges are presented as red dots. Details of these stations are given in Tables 3.1 and 3.2.

Both tide datasets are available at an hourly resolution and each of the records provides the total tide level, which represents the combined influence of the astronomical tide and storm surge. Only the storm surge is of interest for a dependence study because it is attributable to the combined influence of atmospheric pressure and wind anomalies acting on the water body, whereas the astronomical tide is less likely to be associated with rainfall extremes. We note that for this report the 'storm surge' is defined to be equivalent to the tidal residual; it is likely to be a composite of many effects, including barometric pressure effects, wind setup, baroclinic shelf-tide interactions, seasonal and inter-decadal influences and coastally-trapped waves. The astronomical tide therefore has been extracted from the tide level for all tide gauge data using a harmonic analysis described by Pugh (1987), and the residual component has been used for the dependence analysis. Note that although the astronomical tide is not expected to be strongly associated with rainfall, it will have a significant influence on the ensuing flood level; this is discussed further in Section 3.5.

Data from the 15 stations of the ABSLMP can be downloaded from <http://www.bom.gov.au/oceanography/projects/abslmp/data/index.shtml#table>, with further information on data formats, accuracy and other information provided there. Data from the 49 tide gauges maintained by various harbour and port authorities was collected by EngTest from the National Tidal Centre (NTC), a division of the Bureau of Meteorology, and further information on this dataset is available in the accompanying report (EngTest, 2010). Further details on the data, as well as restrictions and qualifications of its use, are provided in (EngTest, 2010).

Table 3.1: Station information from the Australian Baseline Sea Level Monitoring Project

Station ID	State	Town/district	Latitude	Longitude	Start Year	End year	Percentage record missing	Storm tide range (m) ¹	Astronomical tide range (m) ²	Storm surge range (m) ³
IDO71001	QLD	Townsville - Cape Ferguson	19° 16' 38.4" S	147° 03' 30.4" E	1991	2010	2.11	4.261	3.97	1.202
IDO71002	QLD	Rockhampton - Rosslyn Bay	23° 09' 39.7" S	150° 47' 24.6" E	1992	2010	1.67	5.304	5.252	0.878
IDO71003	NSW	Port Kembla	34° 28' 25.5" S	150° 54' 42.7" E	1991	2010	0.62	2.45	2.34	0.654
IDO71004	VIC	Stony Point	38° 22' 19.7" S	145° 13' 28.9" E	1993	2010	1.27	3.705	3.255	1.532
IDO71005	TAS	Burnie	41° 03' 0.3" S	145° 54' 54.0" E	1992	2010	1.87	4.157	4.025	1.36
IDO71006	VIC	Lorne	38° 32' 49.9" S	143° 59' 19.8" E	1993	2010	1.99	3.194	2.629	1.294
IDO71007	TAS	Triabunna - Spring Bay	42° 32' 45.1" S	147° 55' 57.8" E	1991	2010	0.36	2.065	1.859	0.848
IDO71008	VIC	Portland	38° 20' 36.4" S	141° 36' 47.4" E	1991	2010	0.88	1.891	1.646	0.919
IDO71009	SA	Adelaide - Port Stanvac	35° 06' 31.0" S	138° 28' 1.3" E	1992	2010	0.89	3.655	2.703	1.979
IDO71010	SA	Thevenard	32° 08' 56.2" S	133° 38' 28.8" E	1992	2010	0.56	3.364	2.499	2.235
IDO71011	WA	Esperance	33° 52' 15.2" S	121° 53' 43.3" E	1992	2010	0.46	1.899	1.559	1.091
IDO71012	WA	Perth - Hillarys	31° 49' 32.0" S	115° 44' 18.9" E	1992	2010	0.11	2.059	1.353	1.243
IDO71013	WA	Broome	18° 00' 3.0" S	122° 13' 7.1" E	1991	2010	1.22	10.588	10.516	3.025
IDO71014	NT	Darwin	12° 28' 18.4" S	130° 50' 45.1" E	1991	2010	0.12	8.253	8.189	1.423
IDO71015	NT	Groote Eylandt - Alyangula	13° 51' 36.2" S	136° 24' 56.1" E	1993	2010	0.93	3.766	2.224	2.053

¹ Storm tide range defined as the minimum sea level minus the maximum sea level over the period of record – includes astronomical tide and storm surge components

² Tidal range defined as the minimum astronomical tide minus the maximum astronomical tide over the period of record

³ Unadjusted for barometric effect

Table 3.2: Station information from the 49 gauges for which storm tide and storm surge data is available. Information extracted from EngTest (2010).

ID	State	Location	Sensor Type	Start	End	Lat	Long	Source	License obtained for use in ARR P18 study
al	WA	Albany	Float (Handar Logger1)	31/05/1960	31/08/2008	-35.0337	117.8925	Albany Port Authority	N
am	QLD	Port Alma	Radar (shaft encoder)	31/12/1985	31/12/2008	-23.5841	150.8625	Maritime Safety Queensland	Y
bb	QLD	Brisbane	Bubbler	14/11/1957	31/12/2009	-27.3595	153.1734	Maritime Safety Queensland	Y
bg	QLD	Bundaberg	Float	16/02/1966	31/12/2009	-24.7597	152.4015	Maritime Safety Queensland	Y
bm	WA	Broome	Acoustic, Pressure	2/07/1966	31/12/2009	-18.0008	122.2186	Broome Port Authority	Y
bo	QLD	Booby Island	Acoustic	1/01/1972	31/12/2009	-10.6067	141.9267	Maritime Safety Queensland	Y
bt	TAS	Burnie	Acoustic	15/07/1952	31/12/2009	-41.0501	145.9150	TasPorts	Y
bu	WA	Bunbury	Float (Handar Logger)	1/11/1963	31/12/2008	-33.3097	115.6409	Bunbury Port Authority	Y
bw	QLD	Bowen		19/11/1986	31/12/2009	-20.0224	148.2515	Maritime Safety Queensland	Y
by	NSW	Botany Bay		28/03/1983	31/12/2009	-33.9745	151.2113	Sydney Ports Corporation	Y
ca	QLD	Cairns	Float	31/05/1960	31/12/2009	-16.9248	145.7806	Maritime Safety Queensland	Y
cn	WA	Carnarvon	Float (Handar Logger)	8/11/1965	31/12/2008	-24.8989	113.6510	Coastal Data Centre, WA Dept. Transport	Y
cr	WA	Cape Lambert	Float (Handar Logger)	25/09/1972	31/12/2008	-20.5833	117.1833	Coastal Data Centre, WA Dept. Transport	Y
dn	NT	Darwin	Acoustic, Pressure	1/01/1959	31/12/2009	-12.4718	130.8459	Dept. of Planning and Infrastructure, NT	Y
dt	TAS	Devonport	Acoustic	4/06/1965	30/04/2007	-41.1850	146.3627	TasPorts	Y
es	WA	Esperance		10/12/1965	31/12/2008	-33.8709	121.8954	Esperance Ports Sea and Land	Y
fd	NSW	Fort Denison	Acoustic	31/05/1914	31/12/2009	-33.8545	151.2259	Sydney Ports Corporation	Y
fm	WA	Fremantle	Float (Handar Logger)	10/1/1897	31/12/2009	-32.0542	115.7395	Fremantle Ports	Y
gc	QLD	Gold Coast Seaway	Radar	1/01/1987	31/12/2009	-27.9667	153.4333	Maritime Safety Queensland	Y
gd	QLD	Gladstone	Acoustic	5/01/1978	31/12/2008	-23.8317	151.2556	Maritime Safety Queensland	Y
gl	VIC	Geelong	Acoustic	1/09/1965	31/12/2009	-38.0969	144.3864	Victorian Regional Channels	Y

								Authority	
gn	WA	Geraldton	Float (Handar Logger)	31/10/1963	31/12/2008	-28.7763	114.6008	Geraldton Port Authority	Y
gt	TAS	Georgetown	No operating gauge	28/07/1965	31/12/2005	-41.1094	146.8219	TasPorts	Y
hp	QLD	Hay Point	Gas purge, Radar	11/08/1969	31/12/2008	-21.2646	149.3135	Maritime Safety Queensland	Y
ht	TAS	Hobart	NA	31/05/1960	30/09/2007	-42.8841	147.3326	TasPorts	Y
kb	WA	King Bay	Float (Handar Logger)	9/10/1982	31/12/2008	-20.6376	116.7293	Dampier Port Authority	N
ld	VIC	Point Lonsdale	Acoustic	27/11/1962	31/12/2009	-38.2933	144.6148	Port of Melbourne Corporation	Y
lu	QLD	Lucinda Point		6/06/1985	31/12/2009	-18.5219	146.3323	Maritime Safety Queensland	Y
mb	NT	Melville Bay		6/10/1965	5/08/2007	-12.2269	136.6953	Dept. of Planning and Infrastructure, NT	Y
mh	QLD	Mourilyan Harbour	Float	26/12/1984	31/12/2009	-17.5994	146.1252	Maritime Safety Queensland	Y
mk	QLD	Mackay	Radar	1/06/1960	31/12/2008	-21.2667	149.3167	Maritime Safety Queensland	Y
mo	QLD	Mooloolaba	Radar (shaft encoder)	23/07/1979	31/12/2008	-26.6843	153.1329	Maritime Safety Queensland	Y
nc	NSW	Newcastle	Acoustic / Float	1/01/1966	31/12/2008	-32.9240	151.7901	Newcastle Ports Corporation	N
oh	SA	Port Adelaide - Outer Harbour		9/11/1940	31/12/2009	-34.7798	138.4807	Flinders Ports	Y
pa	SA	Port Adelaide – Inner		31/12/1932	31/12/2008	-34.8426	138.4955	Flinders Ports	Y
pk	NSW	Port Kembla	Acoustic/Pressure	24/01/1966	31/12/2009	-34.4738	150.9119	Port Kembla Port Corporation	Y
pl	SA	Port Lincoln	Bubbler	5/06/1964	31/12/2009	-34.7200	135.8750	Flinders Ports	Y
po	VIC	Portland	Acoustic	18/01/1982	31/12/2009	-38.3434	141.6132	Port of Portland	N
pp	SA	Port Pirie	Bubbler	1/01/1941	31/12/2008	-33.1783	138.0122	Flinders Ports	Y
sb	TAS	Spring Bay	Acoustic/Pressure	26/11/1968	31/12/2009	-42.5459	147.9327	TasPorts	Y
sh	QLD	Shute Harbour	Float	31/12/1982	31/12/2009	-20.2932	148.7870	Maritime Safety Queensland	Y
sp	VIC	Stony Point	Acoustic	24/07/1963	31/12/2009	-38.3721	145.2247	Patrick Ports	Y
tl	QLD	Townsville		5/01/1959	31/12/2009	-19.2511	146.8337	Maritime Safety Queensland	Y
tv	SA	Thevenard	Acoustic / Pressure	1/01/1966	31/12/2009	-32.1489	133.6413	Flinders Ports	Y
ur	QLD	Urangan	Radar	25/09/1986	31/12/2008	-25.2764	152.9081	Maritime Safety Queensland	Y
vh	SA	Victor Harbour	Float	13/06/1964	31/12/2009	-35.5624	138.6352	Flinders Ports	Y

wm	VIC	Williamstown		28/01/1966	31/12/2009	-37.8657	144.9165	Port of Melbourne Corporation	Y
wo	SA	Wallaroo	Pressure	15/11/1976	31/12/2008	-33.9257	137.6142	Flinders Ports	Y
wp	QLD	Weipa	Float	27/12/1965	31/12/2009	-12.6700	141.8633	Maritime Safety Queensland	Y
wy	WA	Wyndham	Float (Handar Logger)	17/04/1966	31/12/2008	-15.4500	128.1000	Coastal Data Centre, WA Dept. Transport	Y

Draft for discussion

3.2. Daily Rainfall Records

In this study, a large number of daily rainfall gauges are considered for the dependence study. For each tide gauge, all the daily rainfall gauges that are situated less than 500 km from a tide gauge and with the record length greater than 20 years are selected. Using these criteria, a total of 7,684 daily precipitation stations from across the Australian continent were used for dependence analysis (Figure 3.2).

The daily rainfall is paired with the storm surge event over the common period for dependence analysis. The details of data pairing are given in Section 3.4. The green, blue, yellow and red dots in Figure 3.2 represent daily rainfall stations of the common period with the storm surge between 20-30 years duration, between 30 and 40 years, between 40 and 50 years and records greater than 50 years, respectively. The rainfall stations provide reasonable coverage around the coastal regions for most of Australia, particularly in the populated regions in the east, south and southwest of the continent. In contrast, the coastal regions in the southeastern part of Western Australia and large areas of northern Australia have relatively fewer gauges. The daily rainfall data are maintained by the Australian Bureau of Meteorology, with accumulated rainfall totals recorded in the 24 hours prior to 9am each day.

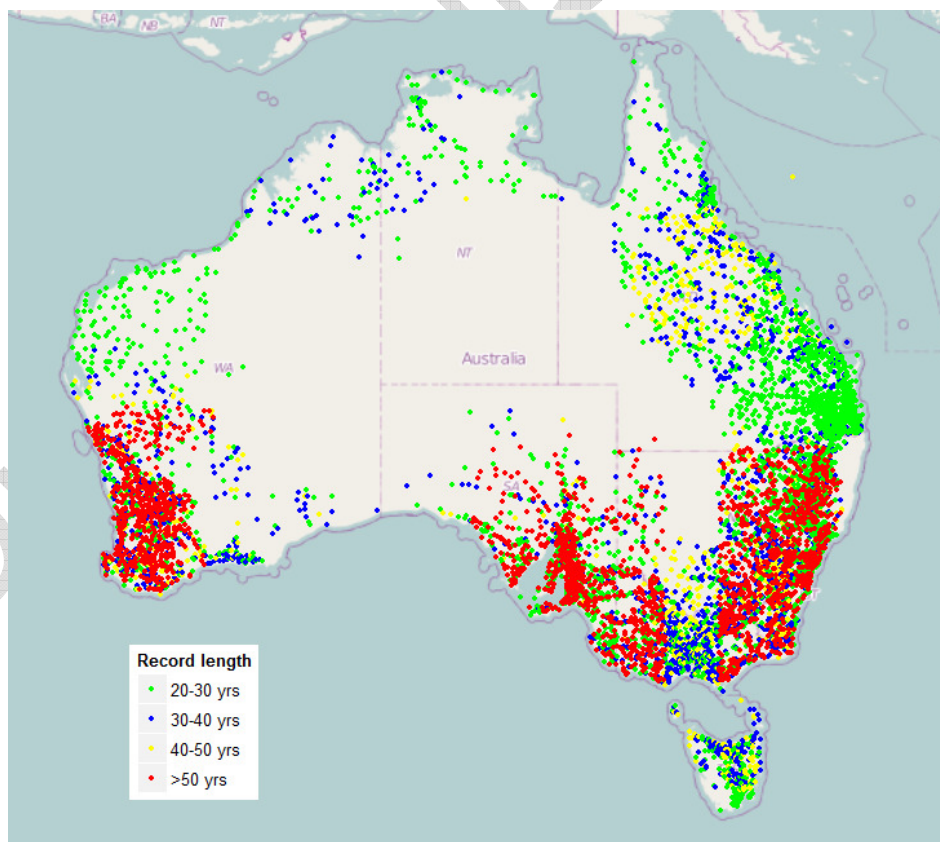


Figure 3.2: Spatial coverage and record length of the Australian daily rainfall gauges. Only locations of the common period with the storm surge > 20 years are presented, totalling 7,684 stations.

3.3. Sub-daily Rainfall Records

The sub-daily rainfall data is used to investigate the variations of dependence as a function of storm burst durations ranging from 15 mins to 168 hours (one week). These sub-daily records are available at a six-minute resolution based on measurements from a combination of Dines pluviographs, Tipping Bucket Rain Gauges and other instruments. This record was provided by the Australian Bureau of Meteorology.

This study used a total of 70 sub-daily rainfall data for dependence analysis and these sub-daily rainfall gauges were selected as they possess relatively longer records and shorter distance to the tide gauge (<200 km). Figure 3.3 present the locations of the 70 sub-daily rainfall gauges, with details given in Table A1 of Appendix A.

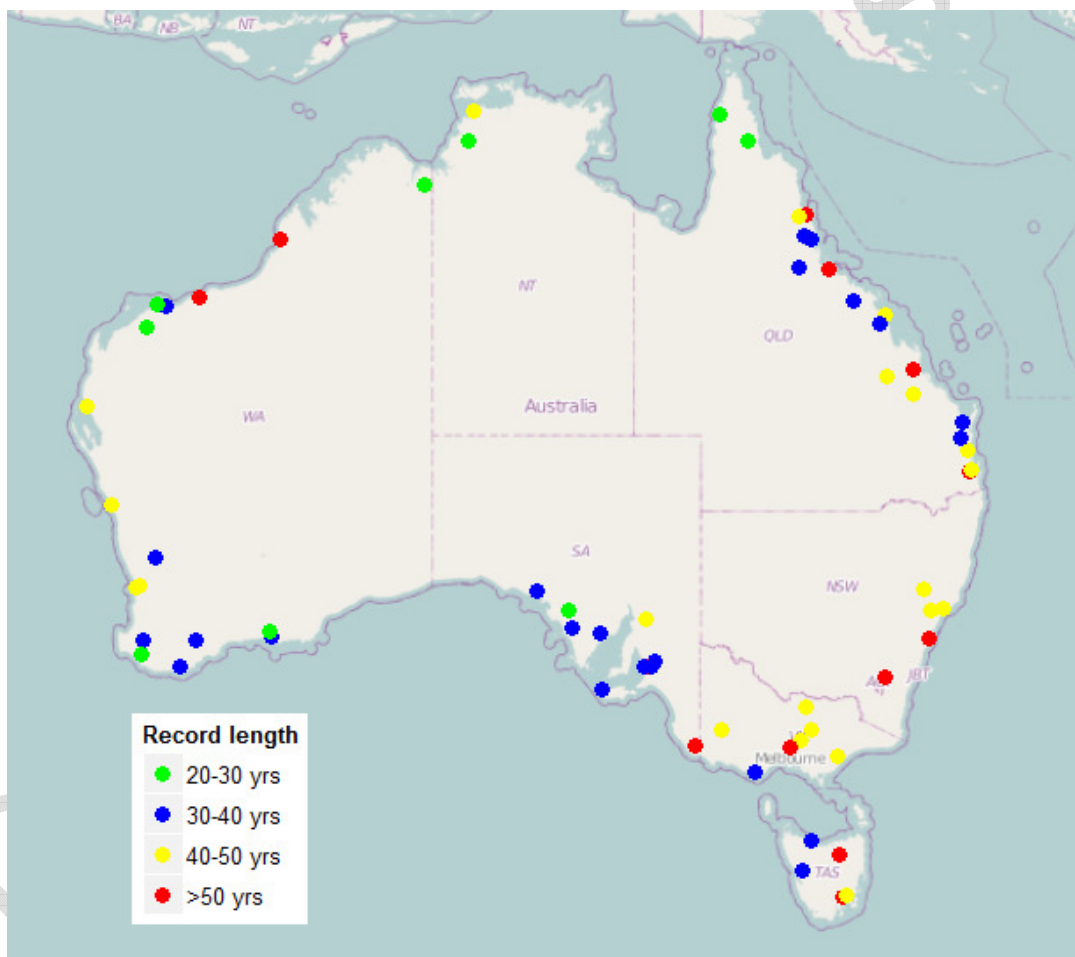


Figure 3.3: The selected 70 sub-daily pluviograph record along the Australian coastline.

3.4. The data paired for the dependence analysis

This section describes the method used for pairing rainfall and storm surge data to enable the dependence analysis. The seven-day storm tide records, astronomical tide levels and their residuals (the storm surges) are all shown in Figure 3.4. Only the storm surge is of interest for the

dependence study because it is attributable to the combined influence of atmospheric pressure and wind anomalies acting on the water body, whereas the astronomical tide is less likely to be associated with rainfall extremes. The storm surge is defined as the residual between the storm tide and the astronomical tide, and is depicted as a red line.

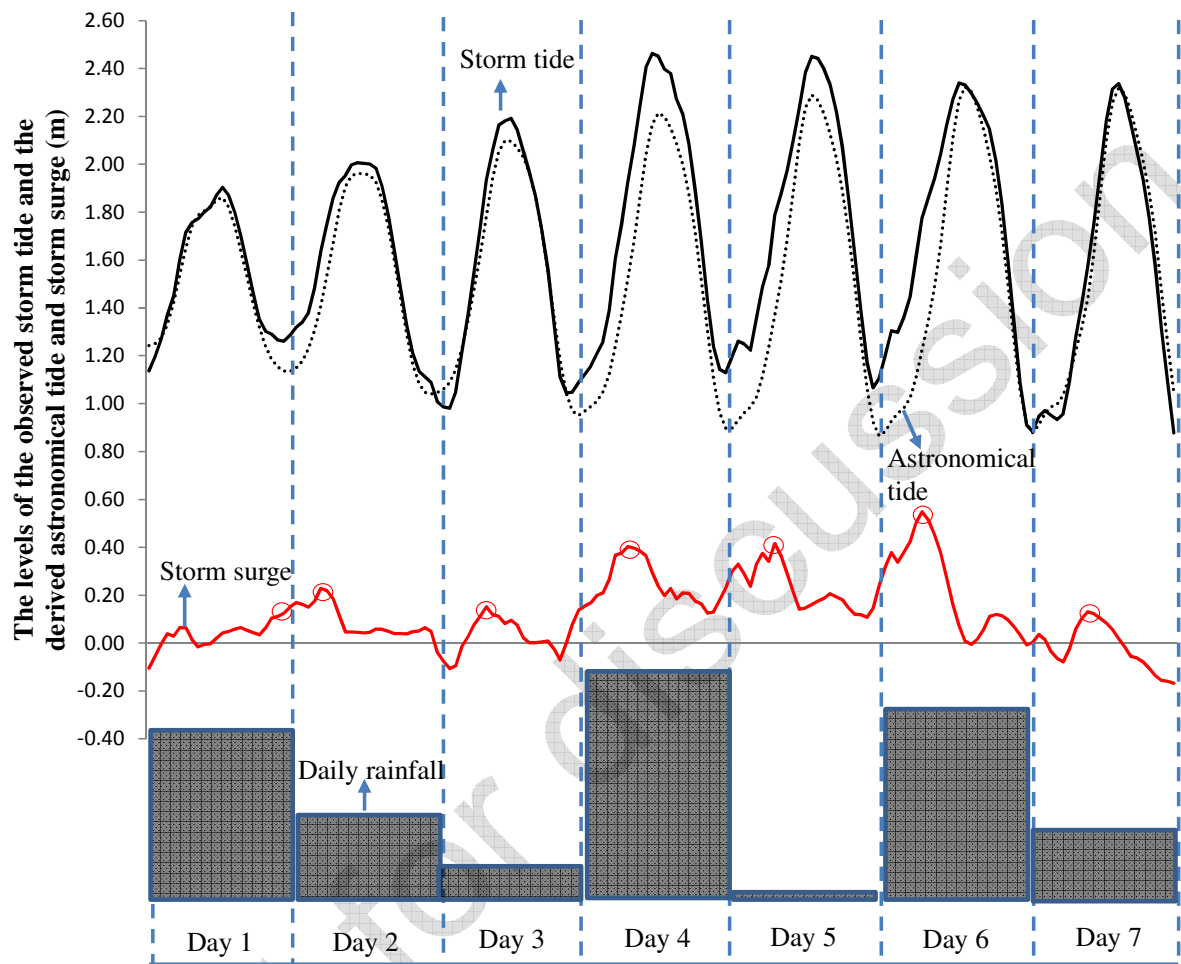


Figure 3.4: An example to illustrate the daily rainfall paired with the daily maximum storm surge. The daily maximum storm surge events are illustrated by the red circles.

The daily maximum value of the storm surge records for each day (denoted by the red circles in Figure 3.4) is paired with the cumulative rainfall over the same 24-hour period (from 9 am to the 9 am) to enable the dependence analysis. A joint extreme event is when the storm surge and rainfall both have a high magnitude on the same day, such as on Days 4 and 6 in Figure 3.4.

To investigate the impact of the storm burst duration on the dependence strength, sub-daily rainfall data were also used. The cumulative rainfall for a given duration is paired with the maximum storm surge over the same duration. For example, if a 48-hour storm burst duration is considered, the total amount of the rainfall is coupled with the maximum storm surge over the same 48 hours as shown in Figure 3.5. The selected pairs then form the basis of the dependence analysis.

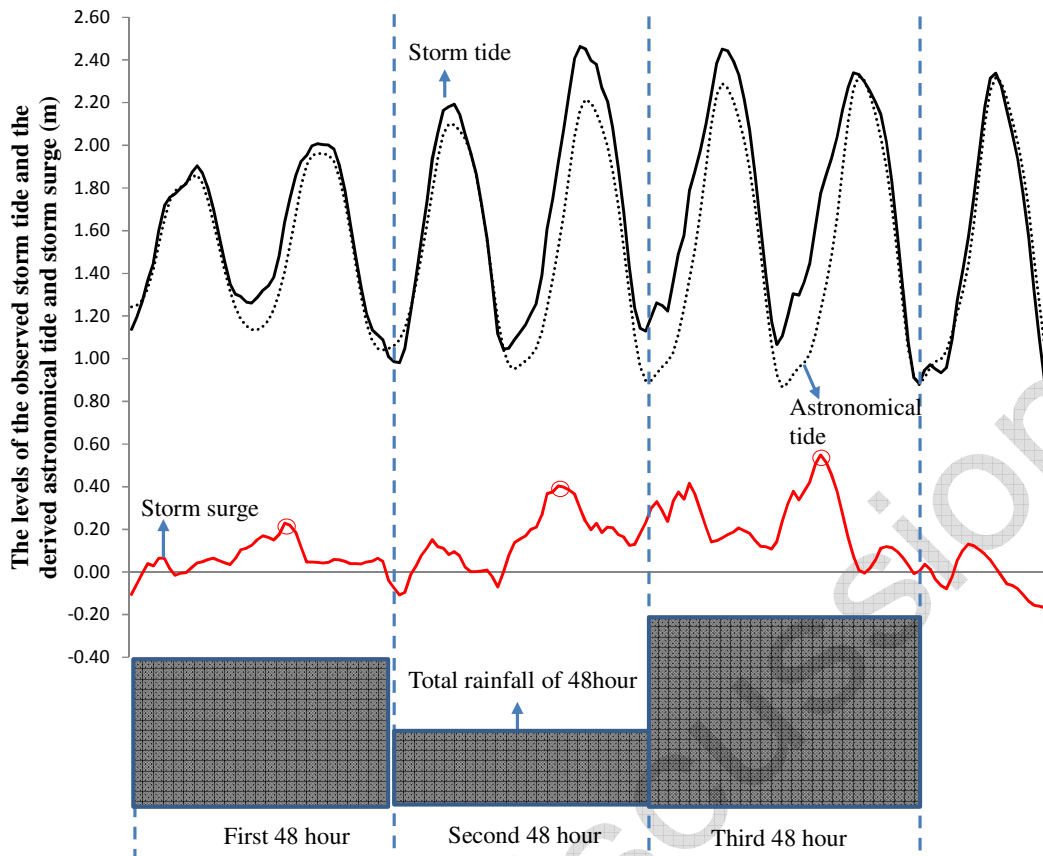


Figure 3.5: An example to show the aggregated sub-daily rainfall paired with the maximum storm surge for a storm burst duration of 48 hours. The maximum storm surge events over the specified storm burst durations are illustrated by the red circles.

The influence of lag between rainfall and storm surge events on the dependence strength was also investigated. For storm burst duration T , the T -hour aggregate rainfall was paired with the maximum storm surge within the T -hour duration either forward or backward in time. For example, a lag of -24 hours using the 24-hour burst duration ($T=24$) represents the dependence of the 24-hour accumulated rainfall paired with the 24-hour maximum storm surge that occurred 24 hours ahead of the rainfall. Taking Figure 3.4 as an example, the daily rainfall on Day 1 is paired with the daily maximum storm surge on Day 2, representing the dependence strength for a lag of $+24$ hours between these two events (i.e., the rainfall event occurs 24 hours ahead the storm surge event). If daily rainfall at Day 2 is paired with the daily maximum storm surge at Day 1, this indicates that the rainfall event occurs 24 hours later than the storm surge event and dependence represents the correlation of these two processes at a lag of -24 hours.

4. Assessment of the asymptotic properties of the joint dependence

There are two categories of extremal dependence: asymptotic dependence and asymptotic independence. Asymptotic dependence represents the case where the dependence between extreme rainfall and storm surge increases as the processes become more extreme. In contrast, if the dependence between rainfall and storm surge becomes weaker as they become more extreme, these two processes are asymptotically independent. Note that asymptotic (in)dependence is a separate concept to dependence at finite levels; for example it is possible to have two variables that are statistically dependent for 'frequent' extreme levels, but that become increasingly independent as the magnitude of the variables increases. Such a process is referred to as being statistically dependent, yet asymptotically independent.

Coles *et al.* (1999) proposed the *Chi* (χ) and *Chibar* ($\bar{\chi}$) plots to assess the asymptotic behaviour between extremes, which are given by:

$$\chi(p) = 2 - \frac{\log \Pr\{F_X(X) < p, F_Y(Y) < p\}}{\log \Pr\{F_X(X) < p\}} \quad (4.1)$$

and

$$\bar{\chi}(p) = \frac{2 \log \Pr\{F_X(X) > p\}}{\log \Pr\{F_X(X) > p, F_Y(Y) > p\}} - 1 \quad (4.2)$$

where F_X and F_Y are the marginal distribution functions of X and Y respectively (X is the extreme rainfall and Y is the extreme storm surge in this study), and p is in the interval $(0,1)$.

The symbols χ and $\bar{\chi}$ are defined as $\chi = \lim_{p \rightarrow 1} \chi(p)$ and $\bar{\chi} = \lim_{p \rightarrow 1} \bar{\chi}(p)$, and together they provide a measure that summarizes the strength of dependence within the class of asymptotically dependent and independent variables. It is observed from Equations (4.1) and (4.2) that, if the increased rate of the joint probability $\Pr\{F_X(X) < p, F_Y(Y) < p\}$ is equivalent to that of the marginal probability $\Pr\{F_X(X) < p\}$ when $p \rightarrow 1$, χ and $\bar{\chi}$ respectively converge to a non-zero value and one (i.e., $\chi > 0$ and $\bar{\chi} = 1$); otherwise $\chi = 0$ and $\bar{\chi} = 0$. For asymptotically dependent variables, $\chi > 0$ and $\bar{\chi} = 1$, with the increase of χ representing the increase in the strength of dependence. For asymptotically independent variables, $\chi = 0$ and $\bar{\chi} = 0$. In practice, replacing probabilities in Equations (4.1) and (4.2) with observed proportions enables empirical estimates of $\chi(p)$ and $\bar{\chi}(p)$.

In this study, daily rainfall was paired with daily maximum storm surge to analyse asymptotic behaviour of extremes along the Australian coastline. Zheng et al. (2013a) have presented an example of $\chi(p)$ and $\bar{\chi}(p)$ using an observed dataset recorded in Brisbane and concluded that interpreting such figures was not straightforward due to their large variance as $p \rightarrow 1$.

In order to resolve this issue, Svensson and Jones (2004) and White (2009) suggested a method to determine the asymptotic behaviour for a given dataset in practice. In this method, a value of χ corresponding to 5% significance level (denoted as χ_s) is first estimated by resampling each margin of the original dataset 1000 times independently in a manner such that dependence is removed. Then the χ value is calculated for each new dataset, resulting in a total of 1000 χ values from which χ_s (5% significance level) could be estimated. A dataset is asymptotically dependent with reasonably strong evidence if its χ value is greater than its 5% significance level (i.e., $\chi > \chi_s$). This method was applied to each of the 49 tide gauges in Table 3.2. The values of χ and χ_s for each tide gauge were obtained by taking the mean of χ and χ_s for all the rainfall/tide-gauge pairs with spatial distance within 30 km. The results are presented in Figure 4.1. In this study, the χ_s value was found to be between 0.03 and 0.04 for all tide gauges.

As shown in Figure 4.1, of the 49 locations, 41 exhibited asymptotic dependence with $\chi > \chi_s$ (red dots). Among those locations, 20 had χ values greater than 0.1, representing strong asymptotic dependence. This shows that the dependence between rainfall and storm surge along the majority of the Australian coastline becomes stronger or at least remains constant as the events become more extreme. These findings have important implications to flood risk analysis, as flood severity caused by jointly occurring extremes is usually greater than when either variable is extreme in isolation.

It is noted that the 15 tide gauges from the ABSLMP (Table 3.1) were not used for asymptotic dependence analysis. This is because (i) the record lengths of these tide gauges are all shorter than 20 years, which are overall significantly shorter than those of the 49 tide gauges in Table 3.2; and (ii) the majority of the tide gauges from the ABSLMP overlap or are very close with those from the second tide dataset (Table 3.2). Given this, the results from 49 tide gauges from the second dataset are suitable to represent the asymptotic behaviours between extreme rainfall and storm surge along the Australian coastline.

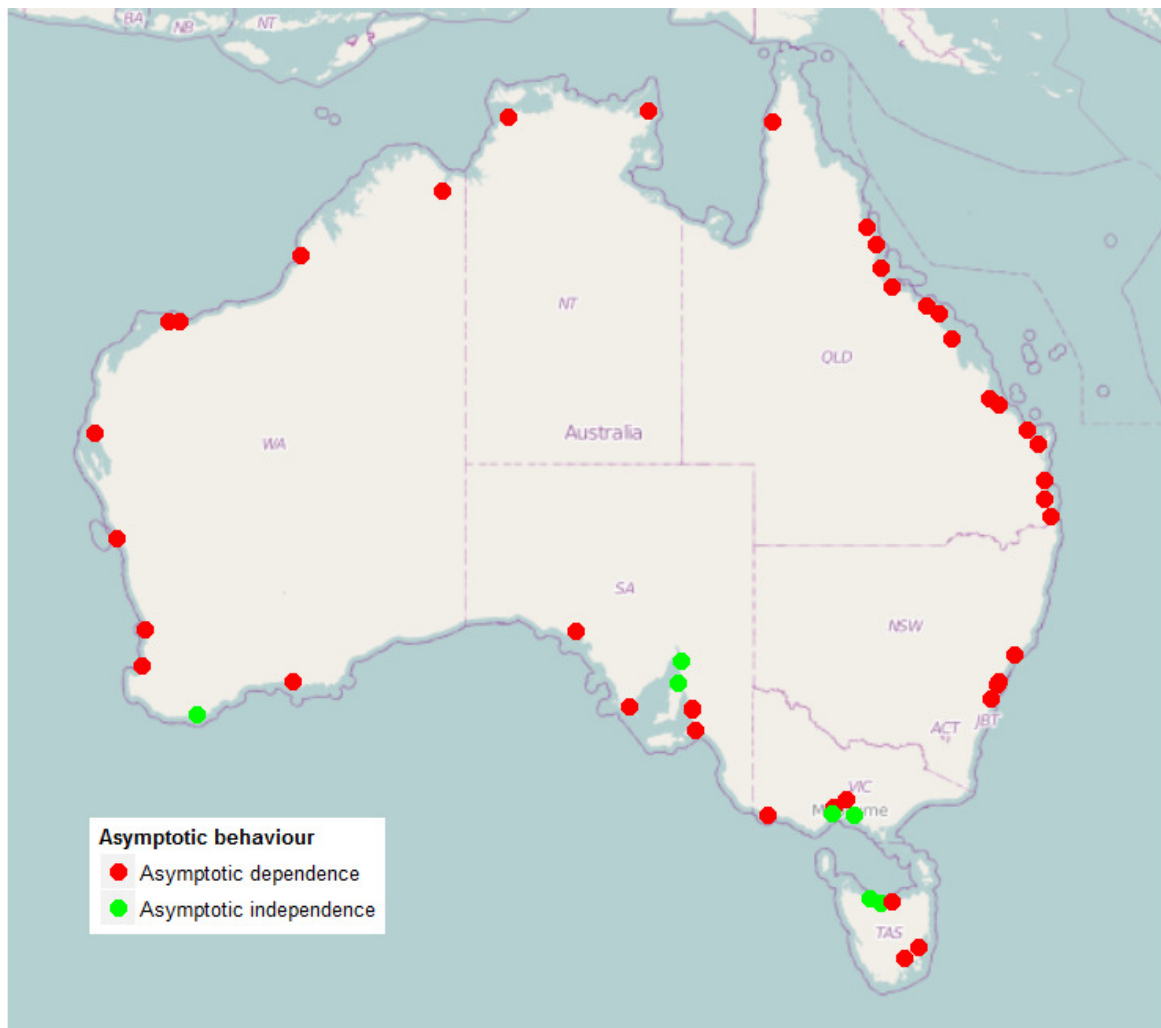


Figure 4.1: The results of asymptotic behaviour analysis for the tide gauges along the Australian coastline. Red and green dots represent the tide gauges exhibiting asymptotic dependence and independence respectively.

Draft

5. Statistical models used for dependence analysis

In this project, we focus on the bivariate extreme value models as only two variables need to be handled. Statistical techniques that are available to represent bivariate extremes are now discussed.

5.1. Representation of bivariate extremes

A variety of methods exist for modelling bivariate extremes and a key distinguishing factor relates to the definition of ‘extreme’. Building on the univariate representations of block maxima and threshold-excess, three mainly distinct representations have been identified: (i) the component-wise block maxima (Tawn 1988); (ii) the threshold-excess method (Resnick 1987); (iii) the point process method (Coles and Tawn 1994). A brief summary of the univariate representation is first described and then their bivariate counterparts are presented.

Univariate block maxima approaches describe the statistical behaviour of:

$$M_n = \max\{X_1, \dots, X_n\} \quad (5.1)$$

where X_1, \dots, X_n , is a sequence of independent random variables having a common distribution function. When $n \rightarrow \infty$, if the limiting distribution of suitably scaled block maxima exists, it converges to the distribution family known as generalized extreme value (GEV) distribution (Jenkinson 1955). In contrast, the univariate threshold-excess model focuses on the distribution of extremes above a suitably high threshold u , with the limiting distribution (if it exists) converging to another family known as the generalized Pareto distribution (GPD), when $u \rightarrow \infty$ (Pickands 1975):

$$G(x) = 1 - \zeta_u \left(1 + \frac{\xi(x-u)}{\sigma}\right)^{-1/\xi} \quad (5.2)$$

where $\zeta_u = \Pr\{X > u\}$, and $\sigma > 0$ and $-\infty < \xi < \infty$ are respectively scale and shape parameters.

The component-wise block maxima representation is a direct analogue of univariate block maxima. Suppose that $(X_1, Y_1), (X_2, Y_2), \dots, (X_n, Y_n)$ is a sequence of bivariate vectors that are temporally independent versions of a random vector (X, Y) . Let $M_{x,n} = \max_{i=1, \dots, n} \{X_i\}$ and

$M_{y,n} = \max_{i=1, \dots, n} \{Y_i\}$, and then define $\mathbf{M}_n = (M_{x,n}, M_{y,n})$ as the vector of the joint extreme events.

The vector \mathbf{M}_n represents the component-wise block maxima. A limitation of this representation is that \mathbf{M}_n will commonly include elements that occurred at different times within a single block,

so that the simulation of component-wise maxima will not necessarily simulate ‘real’ bivariate events. It is also very wasteful of data, as only the maximum values in each block contribute to the analysis. These are severe limitations in practice. As such, the component-wise maxima representation is not discussed further in this research project.

The threshold-excess and point process methods simulate ‘actual’ (i.e. observed) joint events, while differing in the definition of the joint extremes. Figure 5.1 illustrates the extreme representations using the bivariate threshold-excess (left panel) and point process methods (right panel) for a synthetic dataset with unit Gumbel margins. A suitably high threshold has been selected for each margin (u_x and u_y), and extremes that simultaneously exceed both thresholds (blue ‘+’ symbols in Figure 5.1) dominate the dependence strength. In contrast, the point process method handles situations where only a single variable is extreme, as well as when both variables are simultaneously extreme. The point process representation is depicted in the right panel of Figure 1. Here, the data are first transformed to radial ($r = x + y$) and angular ($w = x/r$) components; the extremes are then defined as events that occur above a suitably high radial threshold r_0 (red ‘+’ symbols in Figure 5.1).

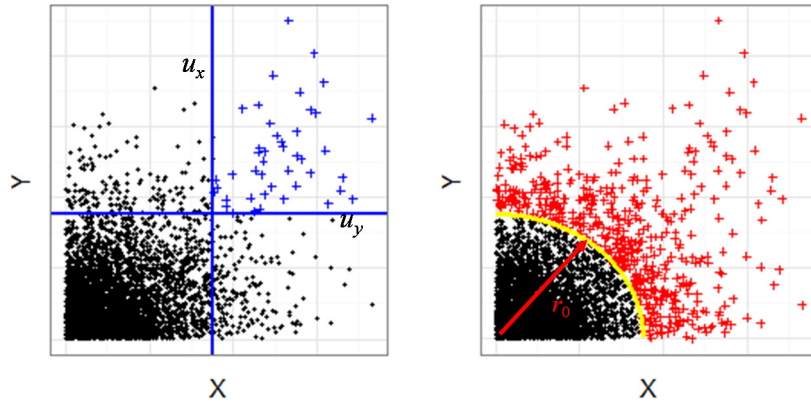


Figure 5.1: Comparison between the representations of “extreme values” using threshold-excess method (left panel) and point process method (right panel).

5.2. Bivariate extreme value theory

In bivariate extreme value theory, the vector \mathbf{M}_n is normalized to $\mathbf{M}_n^* = (M_{x,n}^*, M_{y,n}^*)$, where $M_{x,n}^* = \max_{i=1,\dots,n} \{X_i\} / n$ and $M_{y,n}^* = \max_{i=1,\dots,n} \{Y_i\} / n$, in order to avoid degeneracy of the limiting distribution as n becomes large. The bivariate margins of (X, Y) are also assumed to follow a standard Fréchet distribution, i.e., $F(z) = \exp(-1/z)$, which is easy to achieve through transformation of the empirical cumulative distribution function. Then the limiting bivariate extreme value distribution is given as:

$$\Pr\{M_{x,n}^* \leq x, M_{y,n}^* \leq y\} \rightarrow G(x, y) \quad (5.3)$$

as $n \rightarrow \infty$, where G is a non-degenerate distribution function that satisfies certain homogeneity and mean constraints (Coles 2001).

A number of different parametric families have been developed (Kotz and Nadarajah 2000) to enable the practical application of Equation (5.3). Among them, the logistic model is widely used due to its simple structure and low number of parameters (Tawn 1988):

$$G(x, y) = \exp\{-(x^{-1/\alpha} + y^{-1/\alpha})^\alpha\} \quad 0 < \alpha \leq 1 \quad (5.4)$$

where the parameter α is used to quantify the dependence strength with $\alpha=0$ and $\alpha=1$ representing complete dependence and independence, respectively. A lower (higher) α suggests an overall stronger (weaker) association between the two variables at extreme levels.

de Haan (1985) described the bivariate extreme value distribution using the limiting Poisson process. In his method, the Cartesian coordinates (x, y) are transformed to pseudo-polar coordinates (r, w) , with radius $r = x + y$ and angle $w = x/r$. The r and w respectively provide measures of the distance to the origin $(0, 0)$ and angle on a $[0, 1]$ scale. *de Haan* [1985] proposed to use $H(w)$ to measure the intensity of the angular spread of points in the limit Poisson process, and $h(w)$ to represent the spectral density function of $H(w)$ if it is differentiable, i.e., $h(w) = dH(w)$.

The spectral density function for the logistic model is given as (Coles and Tawn 1994):

$$h(w) = \frac{1}{2} (\alpha^{-1} - 1) \{w(1-w)\}^{-1-1/\alpha} \{w^{-1/\alpha} + (1-w)^{-1/\alpha}\}^{\alpha-2} \quad (5.5)$$

Although the characterization of the bivariate extreme value distribution assumes standard Fréchet margins, this implies no loss of generality as any GEV distribution can be transformed to the standard Fréchet scale.

We illustrate the implication of different values of α using three synthetic datasets generated from the bivariate logistic distribution function with varying dependence strengths: $\alpha=0.1$ (strong dependence), $\alpha=0.5$ and $\alpha=0.95$ (weak dependence). The data are presented in Figure 5.2 where we assume that the data points located in the top 10% of the radial component (r) are extreme (shown as grey dots). It is clear from Figure 5.2 that the smaller α is, greater the number of events that are extreme in both X and Y .

Both the threshold-excess and the point process methods are derived from Equation (5.3), but they differ in their methods of parameter inference and in their definition of joint extremes, as discussed in Section 5.1. We illustrate the differences of the parameter estimation (α) between these two methods using the logistic model given in Equation (5.4). A censored likelihood method is typically used for estimating α for the threshold-excess method, in which the joint extreme data (x, y) such that both $x > u_x$ and $y > u_y$ dominate the dependence strength (the

estimate of α), and the observations that lie below the threshold only provide a censored contribution to the likelihood, regardless of the magnitude of the true values. For the point process model, inference is commonly based on a likelihood function constructed from the spectral density, $h(w)$, given in Equation (5.5), using all data (w,r) such that $r > r_0$ is extreme.

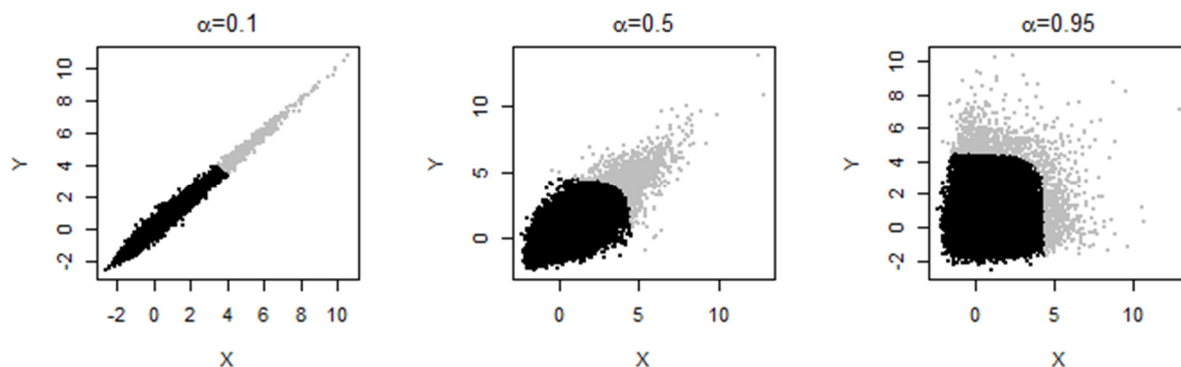


Figure 5.2 Illustration of the dependence parameter α using three datasets generated from the bivariate logistic model ($\alpha=0.1, 0.5$ and 0.95).

It is noted that both the threshold-excess and point process method derived from Equation (5.3) are only valid in some joint tail region where one component is asymptotically dependent on the other component (Coles and Tawn 1994). The analysis in Section 4 showed that the majority of the tide gauges along the Australian coastline exhibited asymptotic dependence (i.e., the dependence remains constant or strengthens as the rainfall and storm surge become more extreme). This implies that both the threshold-excess and point process methods are suitable for quantifying the dependence between extreme rainfall and extreme storm surge for the Australian coastline. The fitting procedures for obtaining the dependence parameter α are presented in Appendix B (see also Zheng *et al.* (2013 b)).

5.3. Selection of bivariate extreme value model

Zheng *et al.* (2013b) conducted a systematic analysis on the performance of the threshold-excess and point process methods, and obtained the following conclusions:

- (1) The threshold-excess model is able to correctly quantify the dependence strength, although the simulation is dominated by joint extreme events in the upper quadrant with all components greater than their corresponding thresholds. In terms of flood risk estimation, events with only one extreme component (such as an extreme rainfall event with no surge or an extreme storm surge event with no rainfall) can also cause floods in coastal catchments. Given this, the practical application of the threshold-excess model is limited.
- (2) The point process method is able to handle all extreme regions since all events with their

radial components greater than a suitably high threshold (r_0) are modelled. However, the point process method produces upwardly biased estimates of the dependence strength, particularly for datasets with weak dependence. For details see Zheng et al. (2013b). As will be discussed in Section 6 of this report, the dependence between extreme rainfall and extreme storm surge along the Australian coastline was statistically significant but weak, with $\hat{\alpha}$ between 0.9 and 0.95 for the majority of the tide gauges. For such weak dependence, the use of the point process method will produce overestimation of the resultant flood risk along the Australian coastline.

To address the issues of both the threshold-excess and point process methods, we investigated the effectiveness of the point process method but with α estimated using the threshold-excess model. The aim of this approach is to minimise the bias in the dependence parameter, while still being able to handle the situation whereby only a single variable is extreme. The results showed that such a hybrid method was able to match observed datasets reasonably well in terms of the number of events in extreme regions, with details given in Appendix C. Therefore, the point process method with parameter estimates from the threshold-excess method is adopted for incorporating dependence into flood risk analysis along the Australian coastline.

Draft for discussion

6. Results of dependence study

6.1. Interpretation of the dependence parameter α

The threshold-excess logistic model was demonstrated in Chapter 5 to be suitable to quantify the dependence between extremes (see also Zheng *et al.* 2013b), and it was therefore adopted for further study of dependence behaviour. Daily rainfall was paired with daily maximum storm surge during the same 24-hour period in order to measure the dependence between these two processes (see Figure 3.4). The threshold-excess logistic model was applied to pairs of rainfall/storm surge data obtained from the 64 tide gauges and all the rainfall gauges that are located less than 300km from the tide gauges and that have more than 20 years of records after pairing with the storm surge data. This yielded 13,414 pairs of daily rainfall and daily maximum storm surge data, as some rain gauges were paired with more than one tide gauge.

We used thresholds on each margin equivalent to the 99th percentile of the observed rainfall and surge data, corresponding to 3.65 joint exceedances per year on average. Given the thresholds, we would expect, on average, one event every $100 \times 100 = 10,000$ days (~ 27.8 years) to exceed the threshold under the null hypothesis that the processes are independent. The thresholds were valid for a large number of locations based on diagnostic plots described in Zheng *et al.* (2013a), and the same threshold percentile was used everywhere to facilitate interpretation and analysis.

To assist with the interpretation, the relationship between α and the number of jointly occurring extreme events which exceed the bivariate threshold is shown in Figure 6.1. The latter measure is model-independent (i.e. it is a count of the number of data points above the marginal 99th percentile thresholds, normalised to a rate per 10,000 days). The figure presents the number of exceedances above the bivariate threshold expressed per 10,000 days of record for each of the 13,414 pairs of rainfall data, plotted against the dependence parameter α .

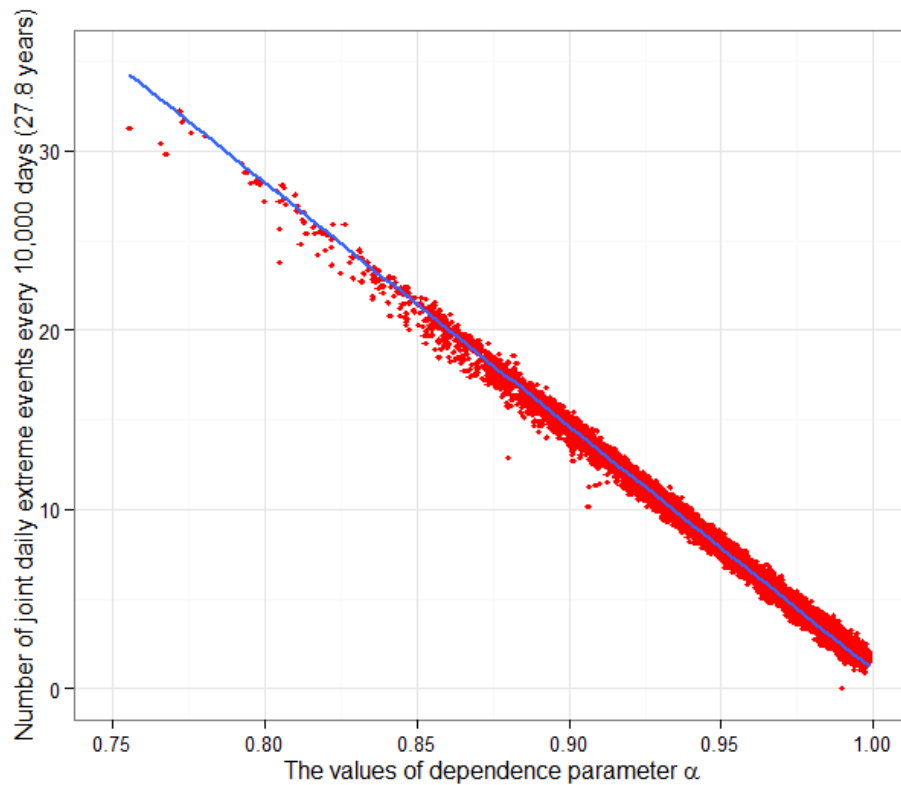


Figure 6.1 The relationship between the dependence parameter α and the number of joint extreme events per 10,000 days (27.8 years).

This figure reveals a clear relationship between the magnitude of the dependence parameter α and the number of observed joint extreme events exceeding the bivariate 99 percentile thresholds, with a lower value of α being associated with a greater number of joint exceedances. This facilitates practical interpretation. For example, a value of $\alpha = 0.95$ indicates approximately 7 events can be expected above the 99th percentile marginal thresholds (compared to one event under the assumption that the two processes are statistically independent), and thus yields a 7-fold increase in the probability of an extreme joint rainfall and storm surge event co-occurring above the threshold compared to the situation where the processes were independent. Similarly, a value of α of 0.9 indicates a 14-fold increase in risk of exceeding the joint thresholds.

6.2. Spatial variation of dependence

To determine the spatial domain of the dependence strength, a large spatial area was considered for each tide gauge. In this study, a square region was established with the tide gauge located in the centre and the area of this square is approximately 1000 km x 1000 km. The common period of the observations between each daily rainfall gauge located within this square and the tide gauge was obtained. All rainfall gauges with the common period greater than 20 years were selected for the dependence analysis.

Figure 6.2 presents the results of four tide gauge locations: Brisbane (Queensland), Fort Denison

(New South Wales), Port Lincoln (South Australia) and Fremantle (Western Australia). These gauges were selected as they represent a diversity of climatic conditions in Australia and possess good coverage of daily rainfall gauges.

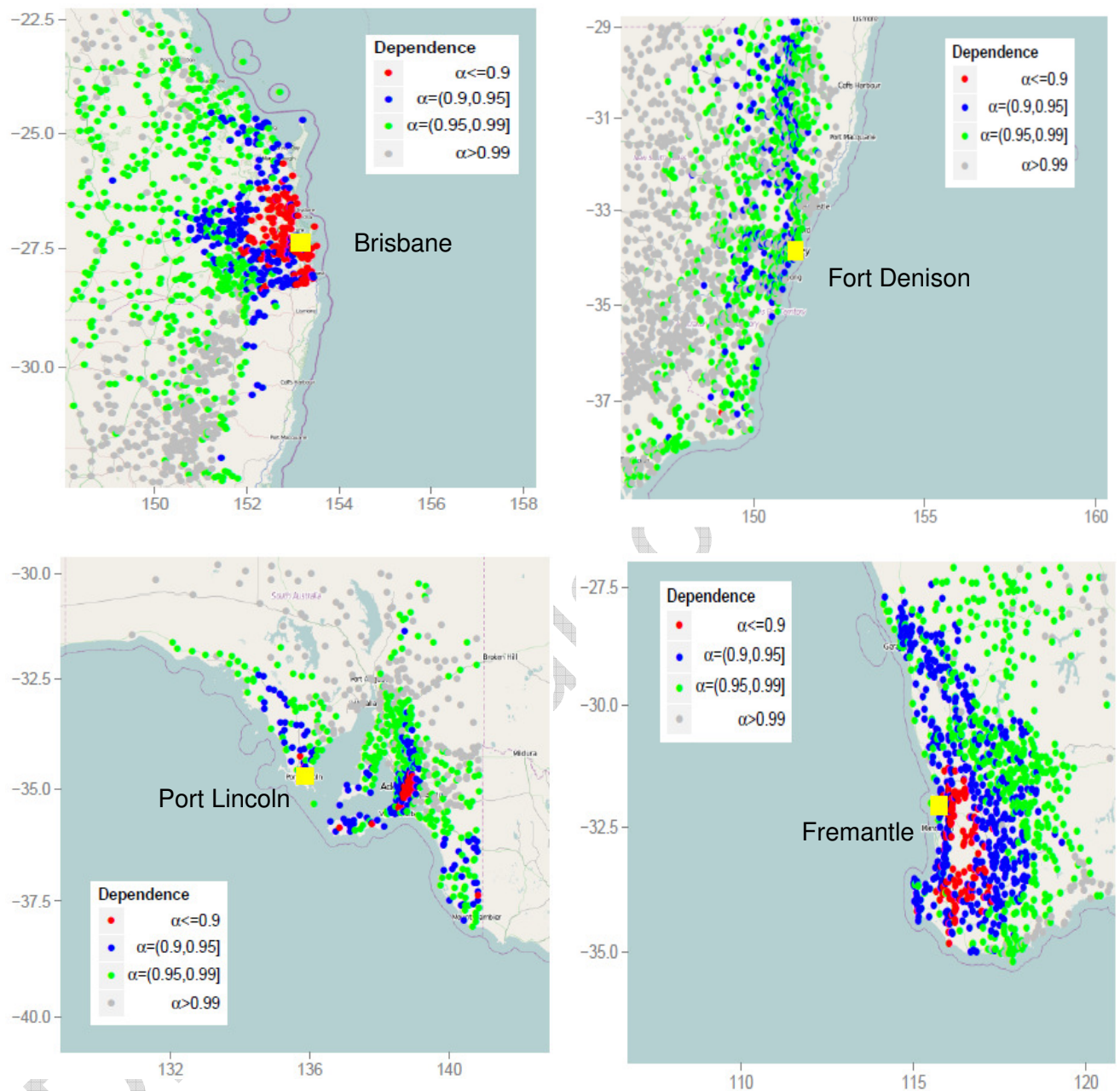


Figure 6.2 The dependence between the daily extreme rainfall and daily maximum storm surge at four locations along the Australian coastline. The yellow squares indicate the tide gauge locations.

Figure 6.2 shows that the distance between the tide gauge and the rain gauge clearly influences dependence strength, with the dependence parameter α overall increasing (and thus the dependence strength decreasing) with longer spatial distance. It is observed that the rainfall stations to the southeast of the Fremantle tide gauge clearly show a greater level of dependence than other areas. This shows that the dependence strength does not change uniformly with

distance to the tide gauge, but is likely to depend on meteorological factors such as the direction of prevailing winds potentially in combination with orographic influences. It is also observed that the rainfall gauges located near the coastline tend to have strong dependence with the tide gauge even for distances up to approximately 500 kilometres. This is because the storm surge normally varies slowly and because rainfall can be correlated over large distances.

The spatial variations of the dependence strength have been investigated for all tide gauges (see Tables 3.1 and 3.2) along the Australian coastline, with results given in Appendix D. The observations of the four example tide gauges in Figure 6.2 are also made for other tide gauges in terms of the spatial variation of the dependence.

6.3. The impact of storm burst duration on dependence

To assess how the strength of dependence changes as a function of the storm burst duration, the dependence parameter was investigated as a function of the storm burst duration at each tide gauge. The results from the four locations used in Section 6.2 are discussed in detail here, with results from the remaining stations provided in Appendix D. Long high-quality records of sub-daily precipitation in the vicinity of the tide gauges were used, and storm burst durations ranging from 15 mins up to 168 hours (one week) were considered. For each storm burst duration, the aggregate rainfall and the maximum storm surge over the duration of the storm burst were paired in order to assess the dependence (see Figure 3.5). The dependence results of various storm burst durations for Brisbane, Fort Denison, Port Lincoln and Fremantle are given in Figure 6.3.

As shown in Figure 6.3, the dependence strength increases (dependence parameter α decreases) when the storm burst duration increases from 15 mins to 24 hours at each of the four tide gauge locations. The strongest dependence for Brisbane and Fort Denison (on the eastern coastline of Australia) was detected for storm burst durations between 48-168 hours (two to seven days), showing that longer-duration rainfall extremes are more closely associated with storm surges compared with shorter-duration rainfall extremes for these locations. Despite some variation caused by the limited availability of long sub-daily rainfall records, the strength of the dependence between extreme rainfall and surge was found to be approximately constant or weaker for burst durations longer than 24 hours at the Port Lincoln and Fremantle tide gauges.

This analysis was repeated for all tide gauges, with details given in Appendix D. Consistent with the results from the four gauges in Figure 6.3, the dependence strength overall increases when the storm burst duration increases from 15 min to 24 hour. When longer storm burst durations were considered (>24 hours), some gauges exhibited stronger dependence and others showed approximately constant or slightly weaker dependence relative to 24 hour durations.

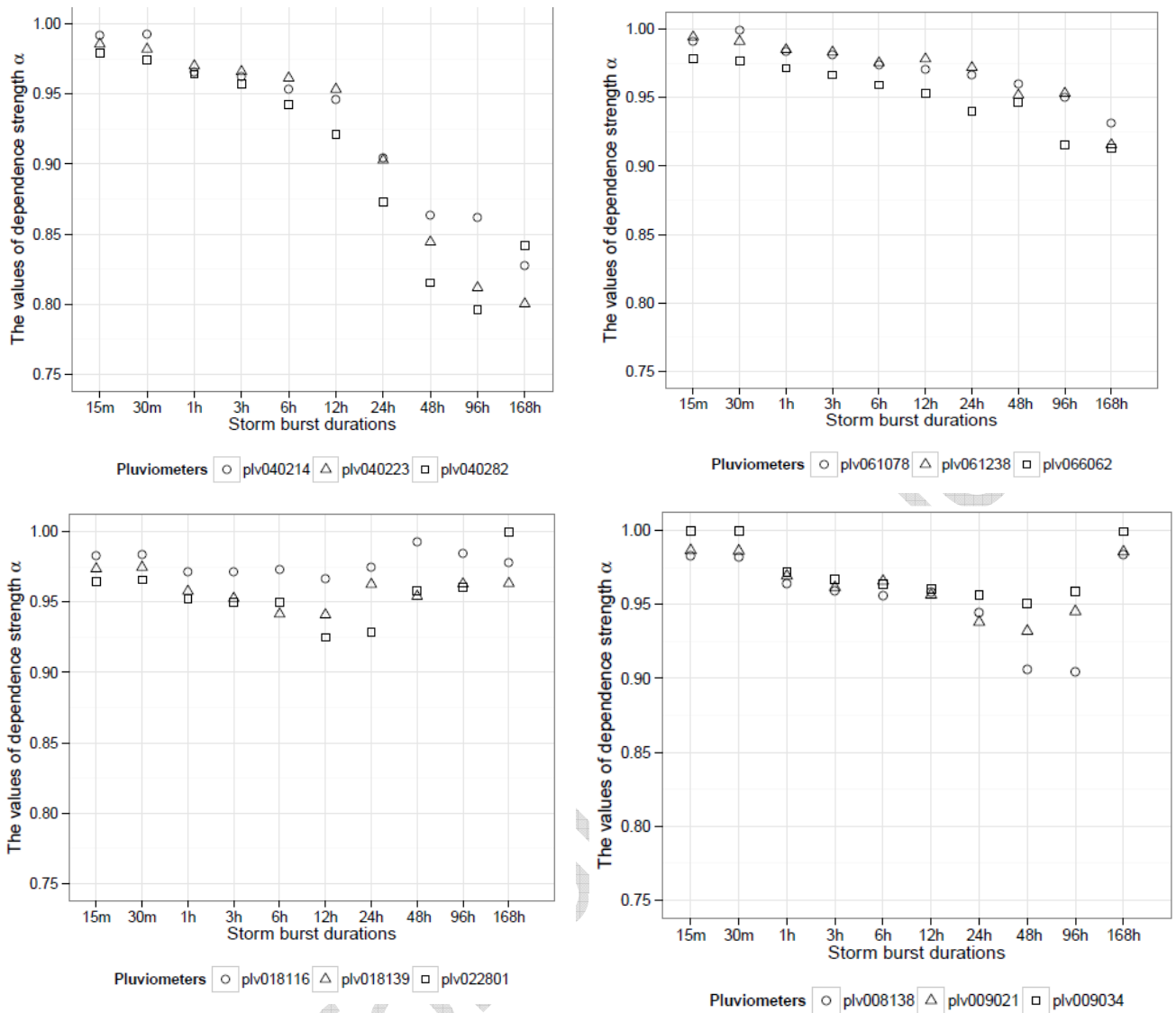


Figure 6.3 Dependence between storm surge and rainfall plotted against storm burst durations for Brisbane (top left), Fort Denison (top right), Port Lincoln (bottom left) and Fremantle (bottom right).

6.4. The impact of lags on dependence

The same data as in Section 6.3 were used to analyse the influence of lags between the rainfall event and the storm surge event on the dependence strength. Storm burst durations of 30 mins, one hour, six hours, 12 hours, 24 hours and 48 hours were investigated. For each duration (T), the T -hour aggregate rainfall was paired with the maximum storm surge within the T -hour duration either forward or backward in time. For example, a lag of -12 hours using the six-hour burst duration ($T=6$) represents the dependence of the six-hour accumulated rainfall paired with the six-hour maximum storm surge that occurred 12 hours ahead of the rainfall. The results for the four illustrative locations are shown in Figure 6.4, with the remaining locations shown in Appendix D.

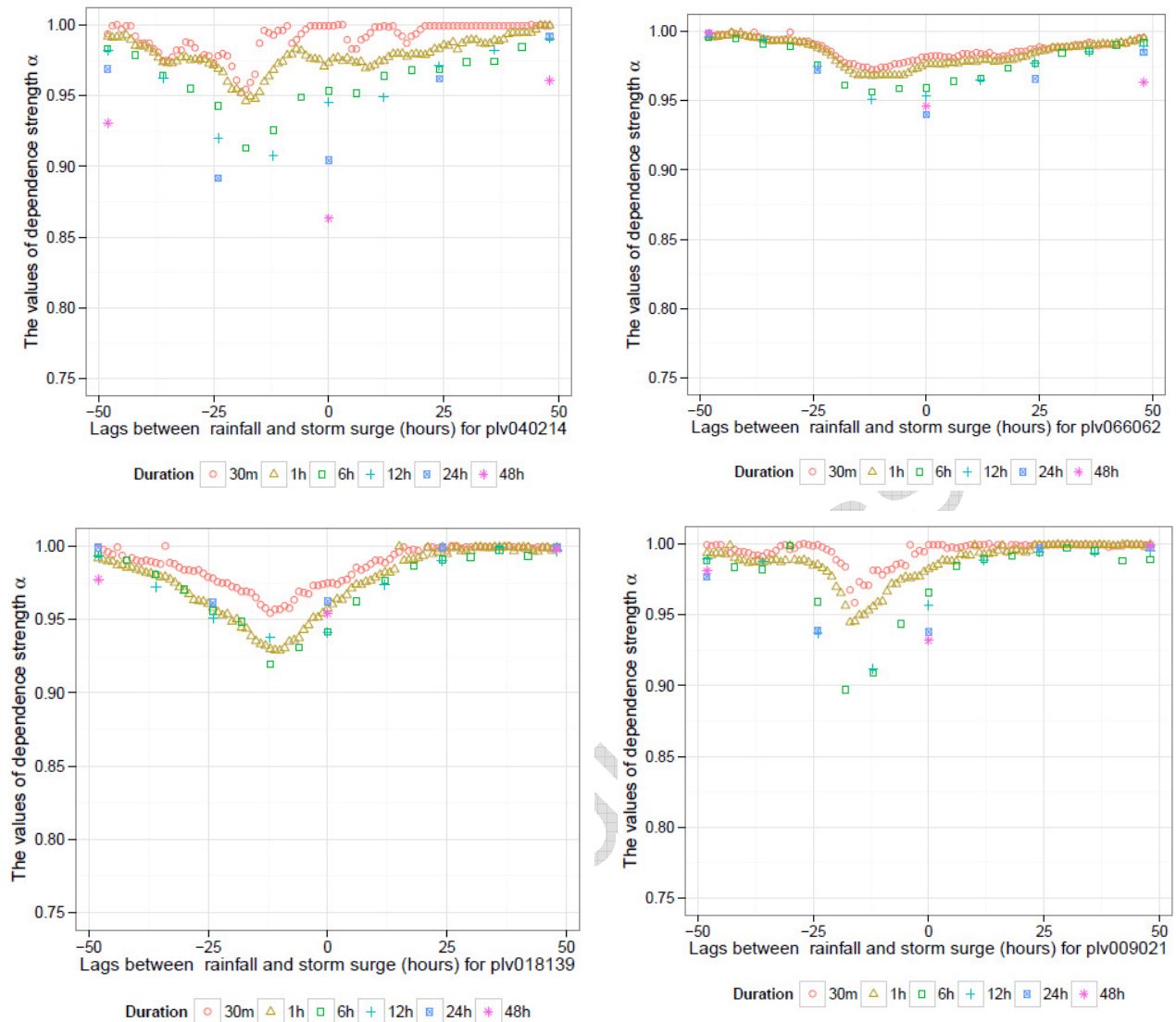


Figure 6.4 Dependence between storm surge and rainfall plotted against lag between extreme rainfall and extreme storm surge for Brisbane (top left), Fort Denison (top right), Port Lincoln (bottom left) and Fremantle (bottom right).

It can be seen that the link between the strength of dependence and the lag varies for different lengths of storm bursts. Interestingly, it was consistently detected that the dependence was strongest when the extreme rainfall was paired with the extreme storm surge that occurred prior to the rainfall event, and this observation was also made for other tide gauge locations.

Figure 6.5 is a schematic to illustrate the impact of lag on the flood risk analysis. We start by assuming that a catchment with a critical duration of six hours is subject to a six-hour extreme rainfall event as shown in Figure 6.5. The peak of the hydrograph is likely to occur towards the end of, or after, the peak rainfall burst due to the time needed for runoff contributions to travel to the catchment outlet. Recall from Figure 6.4 that the dependence is stronger when the lags are negative for six-hour storm burst durations. This suggests that the storm surge events are more

likely to occur at least six hours ahead of the rainfall event, as shown in the red dotted line of Figure 6.5. This implies that the effect of lags (leading to stronger dependence) may have limited impact on the flood risk, as the peak of the storm surge is less likely to co-occur with the peak of the hydrograph. Based on this reasoning (and the consistent observation that at most locations, negative lags produce the strongest dependence), the impact of lags is not further considered as part of the method for estimating flood risk, with all dependence values calculated assuming zero lag (i.e. that the storm surge occurs within the same time increment as the rainfall, such as during the 6-hour rainfall event presented in Figure 6.5). Details of the analysis of lags for each tide gauge are given in Appendix D.

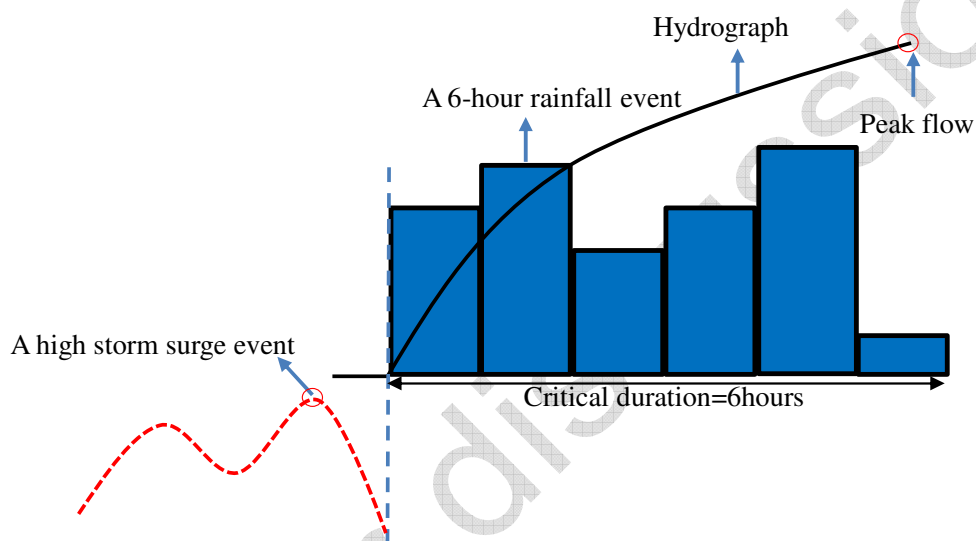


Figure 6.5 An illustration of the implication of the lag between the extreme rainfall and extreme storm surge event on the flood risk.

6.5. Dependence map of the Australian coastline

The results of the investigation into dependence between extreme rainfall and extreme storm surge at all 64 tide gauges are summarised into a single map depicting dependence as a function of the location and the storm burst duration (Figure 6.6). Although there is a site-by-site variation of the dependence strength, our assessment of the results indicates that the stated precision in α should be: (i) averaged at the regional scale; (ii) resolved at increments of no finer than 0.05; and (iii) provided for duration ranges rather than exact durations. These conclusions also greatly simplify practical implementation of the method since the dependence for all cases can be summarised on a single map. Even for the locations that were identified as being asymptotically independent (Figure 4.1), some small level of dependence could be observed at some durations and with some of the rain gauges, and this together with the absence of a clear spatial pattern resulted in the outcome that no regions would be designated as statistically independent. The weakest level of dependence was therefore set at $\alpha=0.98$, with the remaining values spaced at regular increments of 0.05 (i.e. 0.95, 0.90, 0.85 and 0.80).

The dependence values in the map were based on a detailed assessment of results at all the individual tide gauges as presented in Appendix D. A systematic process was provided to convert the individual location results into the Australia-wide map, and a brief summary of the process is given below:

- (1) The 24-hour dependence parameter α for each tide gauge was obtained first by taking the mean value of α for all the daily rainfall gauges with a distance less than 30 km from the tide gauge. This distance was selected as it is likely to encompass the set of daily rain gauges that are located inside catchments that discharge near the tide gauge.
- (2) For storm burst durations T shorter than 12 hours, the dependence results using the sub-daily rainfall data were used for each tide gauge. Based on the results, it can be reasonably justified (given the variability in the data) that the dependence strength with storm burst durations from 15 mins to 12 hours ($T < 12$ hours) can be represented by a single dependence parameter for simplicity due to their similar dependence strength for each tide gauge. The sub-daily rainfall gauges used in the analysis are summarised in Appendix A.
- (3) The dependence parameter obtained using the daily rainfall datasets was used to represent the dependence strength for storm burst durations between 12 hours and 48 hours for each tide gauge ($12 \text{ hours} \leq T \leq 48 \text{ hours}$). This is because the dependence strength was similar across this duration range based on results of dependence analysis using the sub-daily rainfall gauges.
- (4) To minimise sampling variability, we used the daily rainfall data to analyse durations between 48 hours and 168 hours ($48 \text{ hours} < T \leq 168 \text{ hours}$) as the daily rainfall gauges have longer records than the sub-daily gauges. The results from the sub-daily rainfall gauges were also used to aid the determination of a single α to represent the dependence strength for each tide gauge over this range of durations.
- (5) Based on (1) to (4), three values of dependence parameter α were determined for each tide gauge, representing the dependence strength for storm burst durations shorter than 12 hours ($T < 12$ hours), between 12 and 48 hour ($12 \text{ hours} \leq T \leq 48 \text{ hours}$) and between 48 and 168 hour ($48 \text{ hours} < T \leq 168 \text{ hours}$). Following the reasoning outlined in Section 6.4, it was concluded that considering the lagged timing of peaks is not justified, so that only the results for zero lag were considered.
- (6) The values of α for all tide gauges in each region were taken into account to determine a single parameter α for each of the three storm burst duration ranges. The regions correspond to the basins determined using Australian Hydrological Geospatial Fabric (Geofabric) from Bureau of Meteorology.
- (7) The location of the tide gauge was taken into consideration when weighting the individual gaged values to develop the regional parameter, since it is possible that some of the dependence strength can be attributed to specific effects at the gauge location. For

example, for gauges located at the mouth of a river, a ‘tidal residual’ could consist of riverine flows as well as storm surges, thus inflating the estimate of the dependence between extreme rainfall and storm surge. These gauges were assigned lower importance in the overall weighting, and only interpreted in the context of gauges that did not suffer from possible riverine flow contamination. The location of each tide gauge can be seen from the figures in Appendix D.

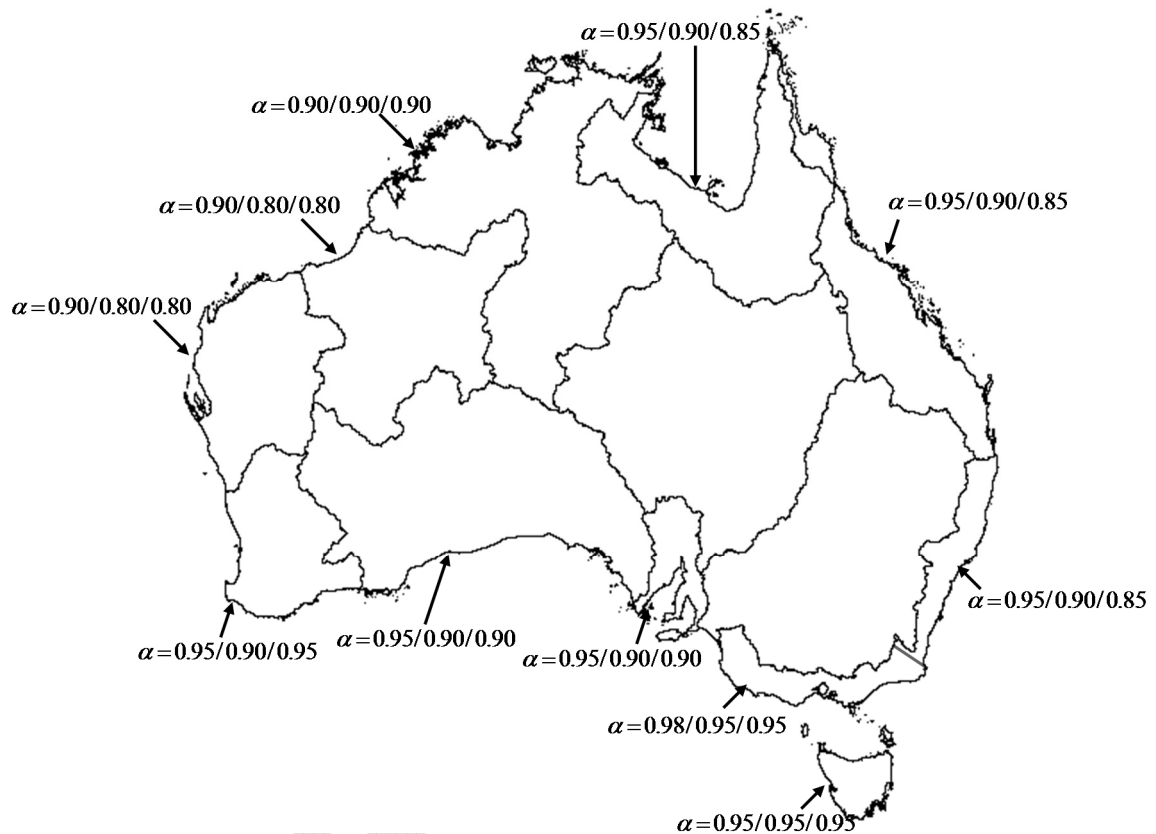


Figure 6.6. The dependence map for the basins of the Australian coastline. The three values of the dependence parameter (α) separated by the slash represent the dependence strength for storm burst durations shorter than 12 hours, between 12 and 48 hours, and between 48 and 168 hours, respectively. Values closer to 1 represent weaker dependence, and values closer to 0 represent stronger dependence.

7. The method used for incorporating dependence for flood risk analysis

The structure function method (referred elsewhere in this report as the “design variable method”) described in Coles and Tawn (1994) was adopted due to its advantage over other methods (such as the 'structure variable method' proposed by Bortot et al., 2000) in terms of the computational efficiency. Following the methodology of Coles and Tawn (1994), the quantity of interest is the exceedance probability of a ‘design parameter’ v , where this parameter is influenced by more than one physically distinct – but potentially dependent – constituent process. In this study, v is assumed to be the design flood level at some location of interest, but it could equally refer to a range of other variables that can be used for engineering design, such as flood flow rate or some other flood parameter. It is further assumed that the primary factors influencing flood level will be a combination of precipitation-induced flows from the catchment (X), and storm tide affecting the downstream boundary (Y). A ‘failure region’, A_v , is defined in terms of these two constituent processes, as follows:

$$A_v = \{(x, y) \in \mathbb{R}^2: b(x, y) > v\} \quad (7.1)$$

where $b(x, y)$ is referred to as the ‘structure function’ (also known as a ‘boundary function’) that translates the two-dimensional input data to a one-dimensional variable of interest such as the flood level. Such a function may be a simple functional such as $v = x + y$, or much more complex.

In engineering practice, flood levels are typically estimated using a combination of hydrologic and hydrodynamic models, and thus in this context $b(x, y)$ represents the output from these models for different values of x and y . The failure region A_v therefore can be interpreted as the set of values of the constituent processes (x, y) that cause the flood levels to be greater than the specified design flood level v , using the transformation between constituent processes and flood levels as contained in the functional $b(x, y)$. The objective of this analysis is to find $p = \Pr\{(x, y) \in A_v\}$; in other words, the probability that the rainfall and storm surge is contained within the failure region A_v , corresponding to the flood level being greater or equal to the design level v . The inverse problem is also often of interest: namely, finding the flood level v that will be exceeded at a given probability p . For example we may wish to know the value of the flood level that has a 1% Annual Exceedance Probability (AEP).

Figure 7.1 illustrates the structure function method with a very simple structure function $v=x+y$, where x and y are two potentially dependent variables. In practice, the exceedance probability of the design variable above a particular value is often of interest, for example $\Pr\{v>10\}$ in the example of Figure 7.1. In the context of the joint probability analysis, there are many different

combinations of x and y can produce $v > 10$ (i.e. failure region A_v) as shown by the filled region in the figure. In the structure function method, the boundary for which $v = 10$ needs to be determined (the red line) first. Then $\Pr\{v > 10\}$ is used to represent the total probability of all different combinations of x and y such that $v = x + y$ is greater than $v = 10$.

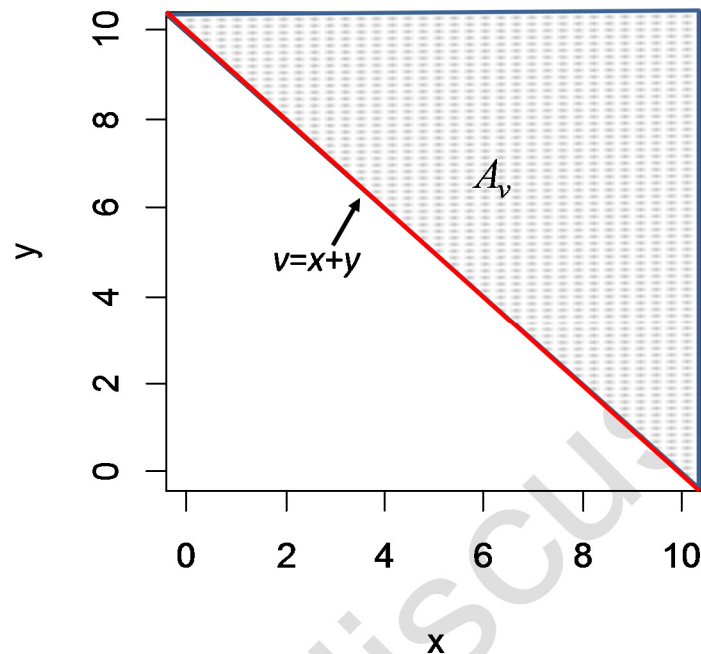


Figure 7.1: Illustration of the boundary function method. v is the design variable of interest influenced by two physically distinct – but potentially dependent – constituent processes (x and y). The red line is the boundary defined by $v = x + y$ and $v = 10$. The filled region represents the events with $x + y$ greater than $v = 10$ (i.e. the failure region A_v).

Although this example uses a simple structure function, the application to more complex engineering design problems follows a similar approach: (1) identify the set of combinations of rainfall and storm surge (or storm tide) that causes the flood levels to exceed a specified design flood level, and (2) assess the probability of that set of events, by accounting for the dependence between extreme rainfall and storm surge as described in the previous section. Combining these two concepts leads to the recommended methodology for calculating flood risk in the Australian coastal zone, which is described further in the following section.

8. Recommended guidance to be included in Australian Rainfall and Runoff

The dependence between rainfall and storm surge as a function of the spatial distance, storm burst duration and lag has been analysed, and the outcome of the analysis is a dependence map that can be used to determine the dependence parameter at any location along the Australian coastline. The dependence parameter for each of the three storm burst duration ranges: shorter than 12 hours ($T < 12$ hours), between 12 hours and 48 hour ($12 \text{ hours} \leq T \leq 48$ hours) and between 48 hours and 168 hour ($48 \text{ hours} < T \leq 168$ hours) is included in the map. The structure function (or design variable) method (see Chapter 7) was then described as a method of estimating flood levels at specified exceedance levels using this information on dependence.

It is acknowledged that incorporating the joint dependence between rainfall and storm surge represents an increase in the complexity of the flood estimation methodology. A pre-screening analysis therefore should be conducted to identify whether joint dependence should be considered for a given situation. Such an analysis ensures that joint probability modelling as described in this report is only conducted for cases where the impacts are likely to be important. Based on the results of this study, a flowchart (Figure 8.1) has been developed as guidance for considering joint dependence in Australian Rainfall and Runoff, with details of each step given below.

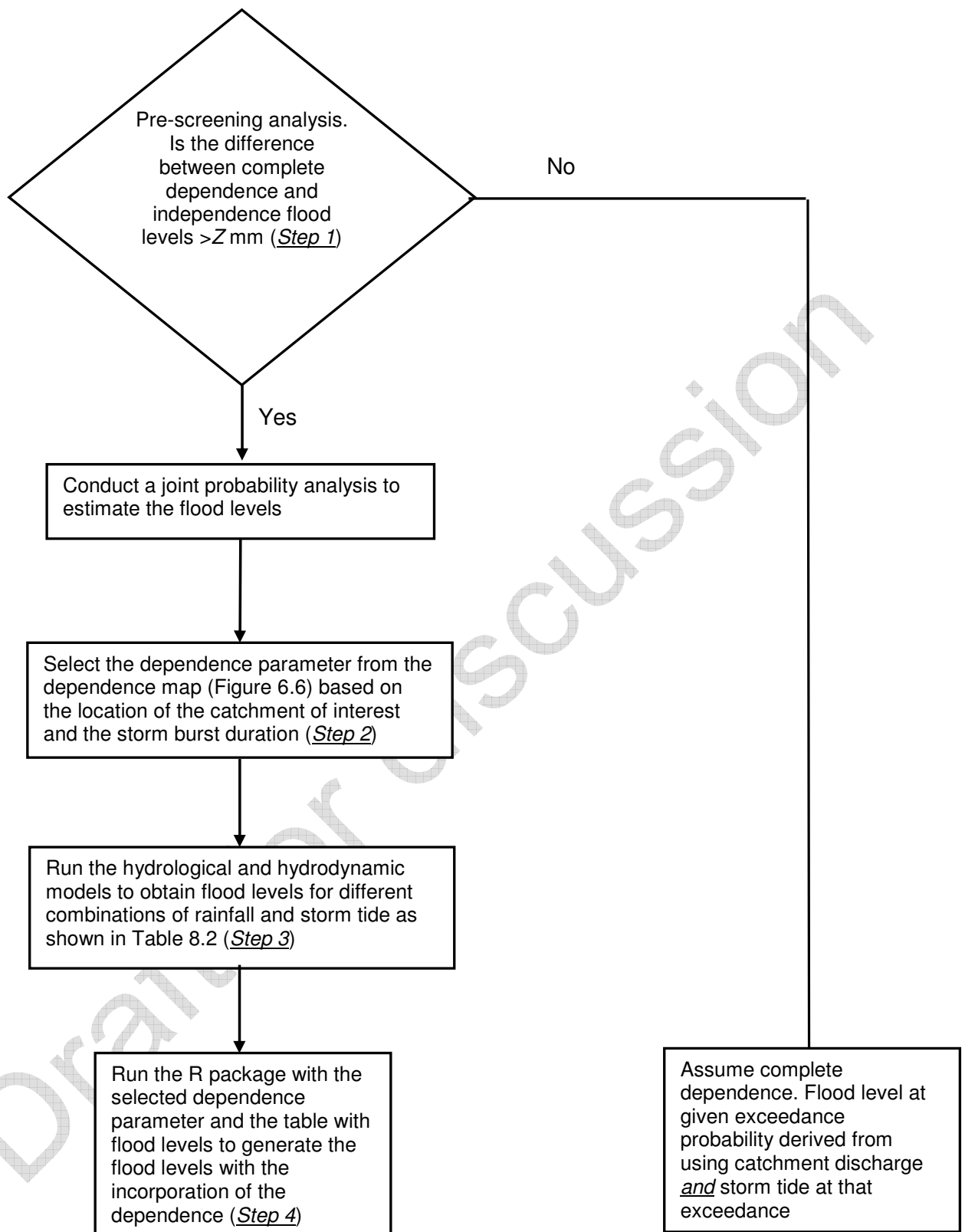


Figure 8.1: Guidance for considering joint probability analysis. The value of Z is user-defined based on an accepted tolerance for the given type of flood study.

Step 1: Pre-screening analysis

The method of incorporating joint dependence represents significant additional computational effort when compared to traditional methods of flood risk estimation. Therefore, a preliminary analysis is recommended to determine whether the additional complexity is warranted for the location being considered. This analysis uses the minimum number of cases to determine the magnitude of flood differences between independence and full dependence. The guidance is based on a tolerance threshold of Z mm described further below.

Table 8.1 identifies nine instances where hydrological and hydrodynamic models need to be run to represent the three separate cases. The grey cells represent water levels caused by extreme rainfall combined with the lowest astronomical tide, whereas the blue cells represent water levels caused by extreme storm tides with no rainfall. Thus, these levels approximately represent the floods that arise due to complete independence (e.g. where the chance of an extreme rainfall event co-occurring with an extreme storm surge event is extremely small), and thus represent a lower physical bound for the true flood levels.

Complete dependence (when rainfall of a given AEP always is accompanied by a storm surge of the same AEP) is represented by the red cells. In all cases, these cells will be equal to or greater than the values of both the grey and blue cells. The red cells thus represent an upper bound of the true flood levels.

If the difference between the complete independence and complete dependence cases is small, then there is little value in continuing with a more comprehensive joint probability analysis. In this case, it is recommended that complete dependence be assumed, as this will be the more conservative (i.e. higher) estimate of total flood risk. In contrast, if the difference between complete independence and complete dependence is large, then there is value in conducting a joint probability analysis to obtain a more precise estimate of the flood risk.

The point at which the difference between complete dependence and independence becomes sufficiently large to justify the additional effort of implementing the joint probability analysis will depend on the specific application, and should be based on an assessment of the required accuracy of the method. The threshold will be a trade-off between the benefit of a more accurate assessment of flood risk (the joint probability calculation) and the cost of implementing a joint probability analysis, since the joint probability analysis has additional computational cost and this cost should be proportional to the benefit of the additional precision. This trade-off will vary according to different locations and design problems, and will depend on the significance of the problem and the consequence of misspecifying the risk. The minimum difference between complete dependence and complete independence is given by a user-specified tolerance value of Z mm.

Table 8.1: Flood levels of different combinations of rainfall and storm tide in terms of AEP (years) with a particular storm burst duration. Only the highlighted cells need to be determined.

		Rainfall events in AEPs			
		No	20%	2%	1%
Storm tide events in AEPs	Lowest astronomical tide				
	20%				
	2%				
	1%				

Floods dominated by rainfall processes: These are situations where water levels in the grey cells are greater than those in the blue cells. An additional criterion is imposed that the grey cells are lower than the red cells for each AEP by less than a tolerance of Z mm. For these catchments, the floods are dominated by rainfall processes, and these would usually be catchments in upstream reaches of the river. For this case, complete *dependence* should be assumed: i.e., the AEP of a flood level is obtained using the same AEP for both rain and storm surge (red cells).

Floods dominated by ocean processes: These are situations where water levels in the blue cells are greater than those in the grey cells. An additional criterion is imposed that the blue cells are lower than the red cells for each AEP by less than a tolerance of Z mm. For these catchments, the floods are dominated by ocean processes, and these would usually be catchments in lower reaches of the river near the estuary outlet. For this case, complete *dependence* should be assumed: i.e., the AEP of a flood level is obtained using the same AEP for both rain and storm surge (red cells).

Floods influenced by both processes: If the flood levels in the red cells are significantly higher than those in either the grey and blue cells (i.e., the difference is greater than Z mm), this indicates that the joint dependence has a significant influence on flood level and it will be necessary to conduct a full joint probability method for flood risk analysis.

It should be noted that if one is only interested in a specific AEP (rather than a range of AEPs) then only three runs are required (instead of the nine runs in Table 8.1). For example if only the 1% AEP is of interest, then the three model runs are: (i) an event with 1% AEP rainfall combined with mean sea level, (ii) an event with 1% AEP storm tide combined with no rainfall, and (iii) an event with the 1% AEP rainfall combined with the 1% AEP storm tide.

If a joint probability analysis is required then the procedure continues with the following steps.

Step 2: Dependence parameter selection.

The dependence parameter is taken from the dependence map (Figure 6.6) based on the location of the catchment of interest and the storm burst duration considered.

Step 3: Flood levels modelling with more combinations of rainfall and storm tides.

In this step, the flood level corresponding to a number of combinations of rainfall and storm tide need to be evaluated in order to estimate flood levels incorporating dependence. For estimating AEPs up to 1%, a typical example is given in Table 8.2 having seven cases for each variable leading to 49 overall runs of a hydrodynamic model.

Table 8.2: Flood levels of different combinations of rainfall and storm tide in terms of ARI (years) with a particular storm burst duration.

		Storm tide events in AEPs							
		LAT	50%	20%	10%	2%	1%	0.2%	0.05%
Rainfall events in AEPs	No rainfall								
	50%								
	20%								
	10%								
	2%								
	1%								
	0.2%								
	0.05%								

Step 4: Undertake joint probability calculations

The joint probability method requires the probability distribution of extremes (specified by the AEP levels in Table 2 and the dependence parameter) to be integrated above each flood level contour to yield a probability of exceeding that level. A software package has been developed to perform these calculations. The package currently is currently written in the R statistical computing language, which is open source software, and requires both a table of flood heights (Table 8.2) and the dependence parameter as inputs. For a given AEP, the resulting flood level will lie between the two cases of complete dependence and independence. Where multiple storm burst durations are considered, the analysis is repeated and the maximum value among these is selected (which represents the critical duration). At present the method has been tested for floods with AEPs ranging from 50% to 1%.

9. Case studies

We illustrate the proposed method using two case studies. Case study 1 is a drainage system in Perth, Western Australia, and case study 2 is the Nambucca River catchment in New South Wales. For the two case studies, two assumptions are made: (i) there is a direct correspondence between the exceedance probability of rainfall over the catchment and the exceedance probability of discharge into the drainage system (case study 1) or the river (case study 2); and (ii) as discussed in Section 3.5, the dependence between rainfall and storm surge is considered to be a reasonable reflection of dependence between rainfall and storm tide (being the sum of storm surge and astronomical tide).

9.1. Case Study 1 – The Perth drainage system

The case study describes a drainage system in the Perth metropolitan area which discharges into the ocean. Therefore the capacity of the drainage system during an extreme rainfall event over the catchment would be influenced by elevated tide levels in the lower reaches. This is a small drainage system that contains 21 separate nodes, and the design flood levels are of interest at each node. The aim of the case study is to estimate the urban flood risk after accounting for the joint dependence between extreme rainfall and storm surges.

The Fremantle tide gauge is located in the Fremantle Fishing Boat Harbour at 32° 03' 56.0" latitude south, 115° 44' 53.3" longitude east, and was assumed to represent the downstream boundary of the drainage system. We fitted the observed extreme tide records from the Fremantle tide gauge using the GPD and then estimated tide levels for lower AEPs. The results of estimated tide levels ranging from AEP=50% to AEP=0.2% are presented in Table 9.1.

Table 9.1. The tide level estimates for various AEPs at Fremantle

AEP	LAT ²	50%	20%	10%	5%	2%	1%	0.5%	0.2%
Tide levels (cm) ¹	79	178	189	195	201	207	211	215	220
Tide levels (m AHD)	0.034	1.054	1.144	1.204	1.254	1.314	1.354	1.394	1.444

¹Datum is Chart Datum which is 2.752m below Tidal Benchmark DMH98 (0.756 m Chart Datum = 0.00 m AHD).

²The lowest astronomical tide.

The joint dependence modelling for this case study is illustrated based on the four steps of the proposed guidance described in Section 8.

Step 1: Pre-screening analysis

We performed the joint dependence modelling to estimate the flood risk for this drainage system, and found that the implications of the joint dependence assumptions were sufficient to warrant detailed joint probability modelling.

Step 2: Dependence parameter selection.

Given the location of the drainage system, we took the dependence parameters from the dependence map in Figure 6.6, which were $\alpha=0.95$, 0.9 and 0.95 for storm burst duration shorter than 12 hours ($T < 12$ hours), between 12 hours and 48 hour ($12 \text{ hours} \leq T \leq 48 \text{ hours}$) and between 48 hours and 168 hour ($48 \text{ hours} < T \leq 168 \text{ hours}$) respectively.

Step 3: Flood levels modelling with more combinations of rainfall and storm tides.

We considered a number of storm burst durations ranging from 15 mins to 24 hours for this case study. Flood levels at each of the 21 nodes in the drainage system were estimated. For each node, the largest estimated flood from the different durations represents the design flood level, and this was computed separately for each AEP. This means that a separate flood level table needed to be created for each location at each storm burst duration, and a script in R was used to automate the process. Table 9.2 shows a flood level table for a particular node with a 15 min storm burst duration.

Table 9.2. Flood levels for various combinations of rainfall and tide levels at a location of the drainage system for 15 min storm burst duration

		Storm tide levels (AEPs)									
		(LAT)	63.2%	39.3%	18.1%	9.5%	4.9%	2%	1%	0.5%	0.2%
Rainfall levels (AEPs)	No rain	0.178	0.984	1.054	1.144	1.204	1.254	1.314	1.354	1.394	1.444
	63.2%	0.739	1.307	1.369	1.450	1.501	1.541	1.584	1.614	1.644	1.683
	39.3%	1.004	1.531	1.579	1.646	1.694	1.733	1.780	1.811	1.840	1.876
	18.1%	1.348	1.801	1.847	1.907	1.948	1.982	2.022	2.048	2.073	2.104
	9.5%	1.559	1.981	2.024	2.080	2.118	2.149	2.186	2.211	2.235	2.266
	4.9%	1.842	2.246	2.289	2.345	2.383	2.415	2.453	2.479	2.504	2.536
	2%	2.215	2.609	2.652	2.709	2.747	2.779	2.818	2.843	2.869	2.901
	1%	2.630	3.018	3.062	3.119	3.158	3.190	3.229	3.255	3.281	3.313
	0.5%	3.135	3.523	3.567	3.624	3.662	3.695	3.735	3.761	3.787	3.820
	0.2%	3.975	4.358	4.403	4.460	4.500	4.533	4.573	4.600	4.626	4.659

Figure 9.1 presents the flood level contour of 1.2 m (the red line) which was obtained by interpolation from Table 9.2. To estimate the exceedance probability of such a flood level, i.e., the failure region A_v in Figure 9.1, one needs to integrate the joint density function of the fitted logistic model with $\alpha=0.95$ (blue contours) upwards from this flood level to derive the exceedance probability that this level will be exceeded. This can be repeated for a range of flood levels, and the flood level corresponding to a desired exceedance probability then can be found accordingly.

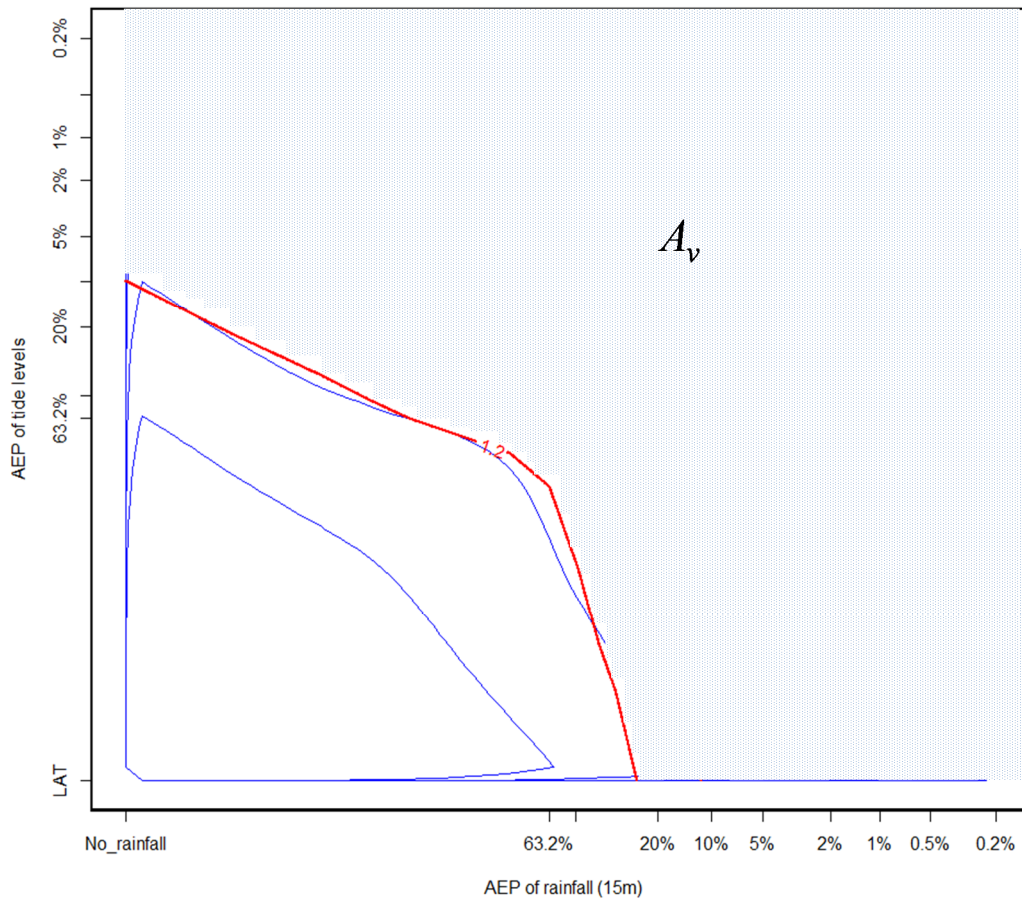


Figure 9.1: The density of the logistic model $\alpha=0.95$ (blue contours), and the water levels for various combinations of rainfall and storm tide events (red lines). The rainfall (15m duration) and storm surge events are given in terms of AEPs. A_v is the failure region that the set of rainfall and storm tides can cause flood levels greater than 1.2m.

Step 4 Undertake joint probability calculations

With the given dependence parameter in Step 2 ($\alpha=0.95$ for $T=15$ min) and the flood level table in Step 3 (Table 9.2), the R package is used to estimate the flood levels for various AEPs (black line in Figure 9.2). In addition, the flood levels under the assumption that the extreme rainfall and storm surge are completely independent (blue dotted line) and dependent (red dotted line) are also presented in Figure 9.2.

As can be seen from Figure 9.2, the flood levels with the incorporation of the estimated joint probability are consistently higher than those obtained under the null hypothesis that there is no dependence (blue dotted line), suggesting that ignoring the dependence between the rainfall and surge would noticeably underestimate the flooding risk for this area.

For each location of the drainage system, we repeated Steps 2 to 4 for each storm burst duration with the dependence parameter selected from Figure 6.6 and the flood level tables obtained in Step 3. For each AEP, the largest value from the estimates using different storm burst durations was selected to represent its corresponding flood levels.

Results from this case study show that although the dependence between rainfall and tidal events at Fremantle is weak ($\alpha=0.90$ or 0.95), it can have significant implications on the flood levels for locations where the water levels are dominated by both the rainfall and tide levels. Ignoring dependence for these locations would dramatically underestimate the flood levels for given AEPs. In contrast, for the locations where water levels are dominated by a single variable (rainfall for upstream locations, or tide levels for downstream locations), considering the dependence does not significantly affect the flood levels.

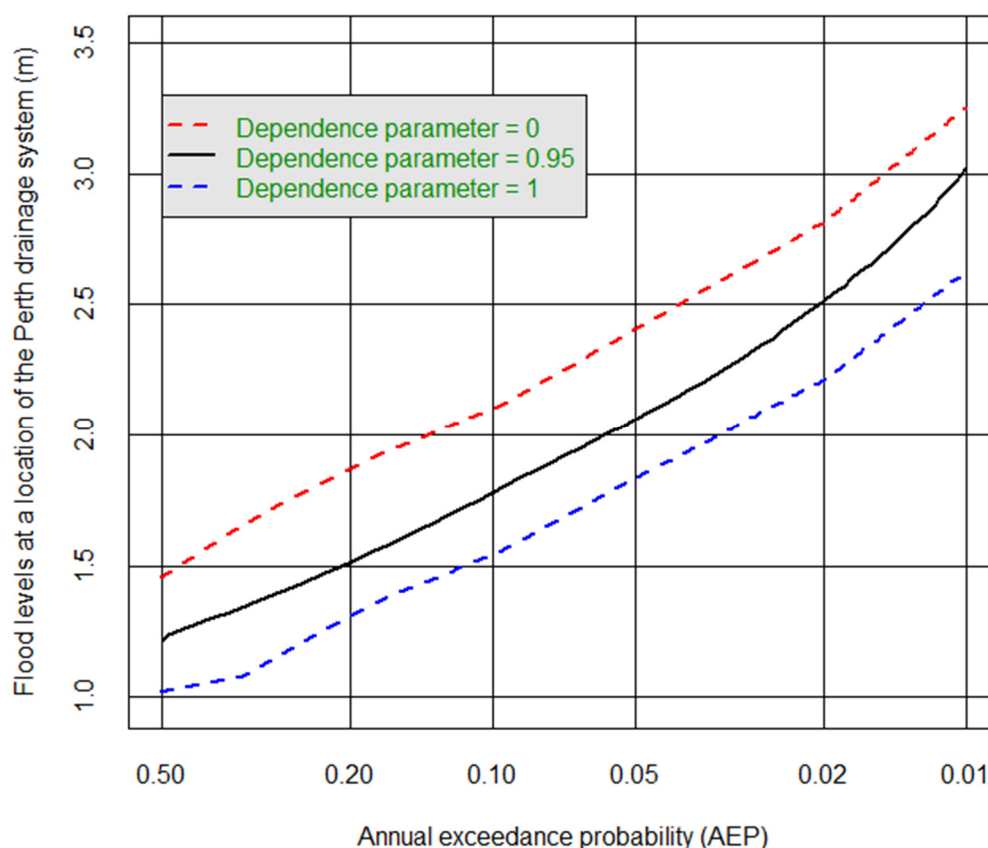


Figure 9.2: Flood levels at a location of the drainage system against different annual exceedance probability (AEPs) for 15 min storm burst durations. Dependence parameters of 0 (red dot line) and 1 (blue dot line) represent the complete dependence and independence respectively

9.2. Case Study 2- Nambucca River catchment

The Nambucca River catchment is located in northern New South Wales. The flood levels in the lower reaches of the Nambucca River are influenced by extreme rainfall over the catchment and extreme storm tides at the ocean boundary. Based on work prepared for the Nambucca Shire Council, modelled flood levels for combinations of boundary conditions were provided from a TufLOW 1D-2D hydraulic model (WMA, 2013). The model is of the Nambucca River, Warrell Creek and tributaries, and covers a catchment area of 1315 km². The model was calibrated to peak flood survey levels (1890-2011) and large historical events (1972, 1977, 2009) recorded at

gauges located at Barraville, Macksville, Stuarts Island and Utungun. Design rainfall data for several locations in the catchment was sourced from Manly Hydraulics Laboratory and the Bureau of Meteorology. A comparison of the design flood levels obtained from the joint probability method with levels obtained from streamflow gaugings was made at the Macksville site due to the long historical record (121 years, 1890-2011) and an additional continuous recording gauge covering the period 1997-2010 (MHL, upstream of Pacific Highway).

The joint dependence method was employed to estimate the flood risk for ten locations, shown as yellow dots in Figure 9.3. These locations cover the downstream, the midstream and the upstream regions of the tidally influenced zone of the Nambucca River. Step 1 (pre-screening analysis) is not relevant to this study as it was already decided to implement a joint dependence method. The analysis moves to subsequent steps of the methodology.

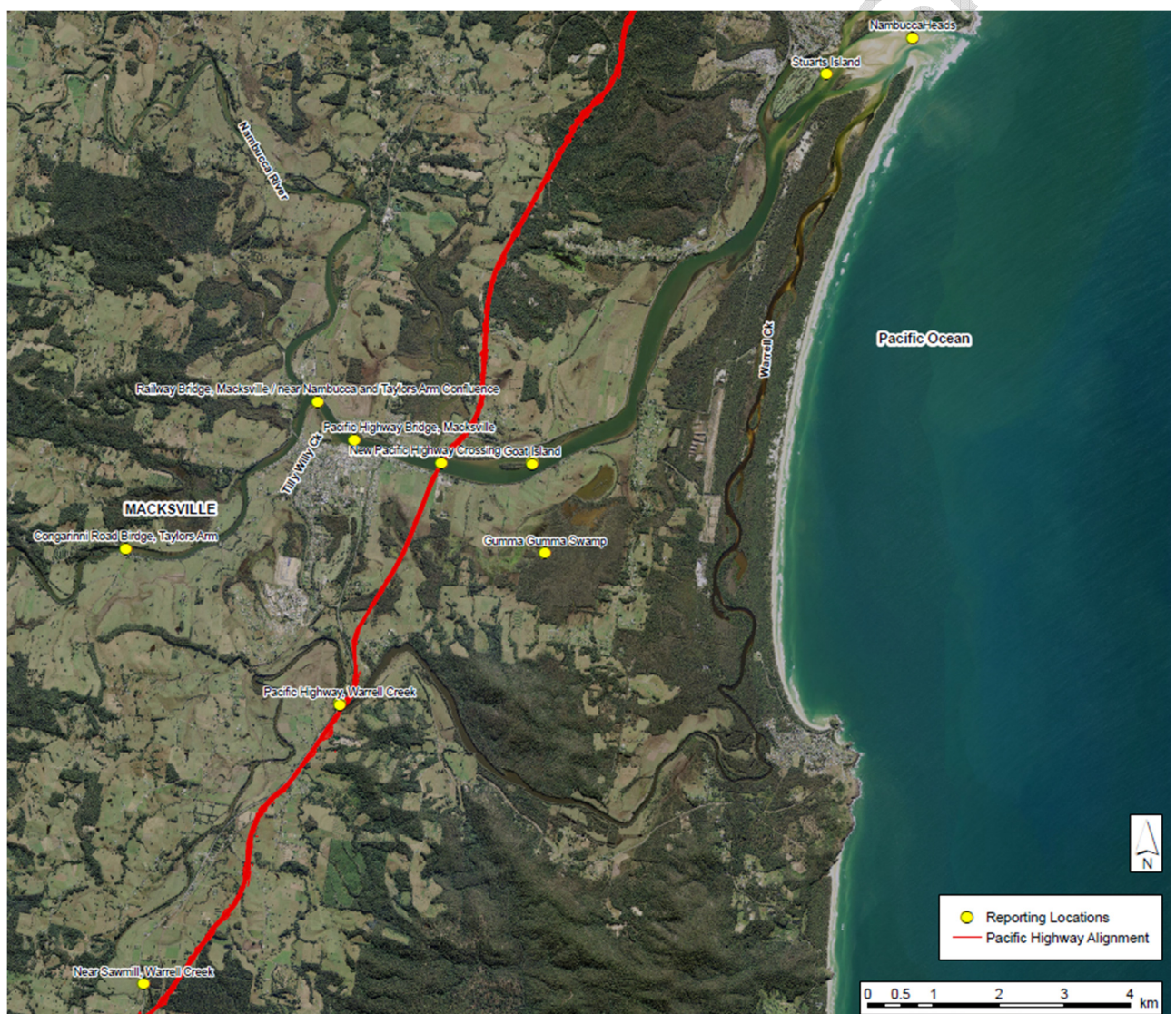


Figure 9.3: 10 different locations considered for Nambucca River catchment (yellow dots)

Step 2: Dependence parameter selection.

The critical duration of the Nambucca River catchment is between 36-48 hours. Given this storm burst duration and the location of the Nambucca River catchment, $\alpha=0.90$, taken from Figure 6.6, was used to represent the dependence between extreme rainfall and storm tides.

Step 3: Flood level modelling with combinations of rainfall and storm tides.

Table 9.3 is a table of flood levels at Macksville for various combinations of critical-duration rainfall and storm tides in terms of AEP. The flood level tables for other locations have also been estimated, but are not shown.

Table 9.3. Flood levels for various combinations of rainfall and tide levels at Macksville (Pacific Highway Bridge) of Nambucca River catchment

		Storm tide levels (AEPs)											
		LAT	63.1%	39.3%	18.1%	9.5%	4.9%	2%	1%	0.5%	0.2%	0.1%	0.05%
Rainfall levels (AEPs)	No rain	0.60	1.35	1.38	1.42	1.45	1.48	1.52	1.55	1.58	1.62	1.65	1.68
	63.1%	1.29	1.70	1.73	1.75	1.77	1.80	1.82	1.84	1.87	1.90	1.92	1.94
	39.3%	1.61	1.92	1.94	1.96	1.98	2.00	2.02	2.04	2.06	2.08	2.10	2.12
	18.1%	1.83	2.08	2.09	2.11	2.12	2.14	2.16	2.18	2.19	2.21	2.23	2.25
	9.5%	2.26	2.43	2.44	2.46	2.47	2.49	2.51	2.52	2.54	2.56	2.58	2.59
	4.9%	2.82	2.96	2.96	2.98	2.98	2.99	3.00	3.01	3.02	3.04	3.05	3.06
	2%	3.32	3.42	3.42	3.43	3.44	3.45	3.46	3.46	3.47	3.48	3.49	3.50
	1%	3.68	3.76	3.76	3.77	3.78	3.78	3.79	3.80	3.81	3.82	3.82	3.83
	0.5%	4.20	4.27	4.27	4.28	4.28	4.29	4.29	4.30	4.30	4.31	4.32	4.32
	0.2%	4.95	4.99	4.99	4.99	5.00	5.00	5.00	5.01	5.01	5.02	5.02	5.03
	0.1%	5.48	5.51	5.51	5.51	5.52	5.52	5.52	5.52	5.53	5.53	5.53	5.53
	0.05%	5.91	5.93	5.93	5.93	5.93	5.94	5.94	5.94	5.94	5.95	5.95	5.95

Step 4 Undertake joint probability calculations

Figure 9.4 shows the flood levels at Macksville (Pacific Highway Bridge) for various AEPs with the incorporation of the dependence parameter ($\alpha=0.90$). The difference between the flood levels for the complete dependence (red dotted line) and complete independence (blue dotted line) is significantly smaller than that in case study 1 (Figure 9.2) especially at rarer flood levels. This implies that one of the flood-producing mechanisms is dominating the final estimates of flood levels, which with further investigation of Table 9.3 was found to be the extreme rainfall (at less frequent AEPs, there is a larger variation with changes in rainfall than with changes in tide).

Figure 9.4 also provides a comparison to flood frequency estimates of stage height based on a GEV distribution fitted to 121 values using the FLIKE software (Kuczera, 1999). The figure shows 90% confidence limits and the expected value at each AEP based on 50,000 Monte Carlo samples. Due to the tidally influenced nature of this location, 93 values below the 2m threshold were censored. Of the 28 gauged values, 1 value, the largest on record, was suggested to have a range 3.5-4m (WMA, 2013). The censoring of this observation was

specified only as being above 3.5m, since the software was unable to specify this value as being within a range. This method was the best way to incorporate the largest flood level as based on many trials (fixed 3.5m, fixed 4m, fixed 3.75m, GEV vs Gumbel distribution) as it was observed that the tail region is very sensitive to the assumptions being made. The GEV distribution was selected over the Gumbel distribution due to the highly skewed shape of the distribution, and the Gumbel distribution significantly overestimated levels at rarer AEPs and had larger uncertainty intervals despite having less parameters. Further inspection of the data and the location would be required to better understand the behaviour of the frequent AEP flood levels. Data from the continuous recording gauge were not used in fitting the GEV distribution but are provided in Figure 9.4 as an alternative source information explaining the frequent AEP flood levels. This gauge shows flood levels which are higher than the lower portion of fitted GEV distribution indicates.

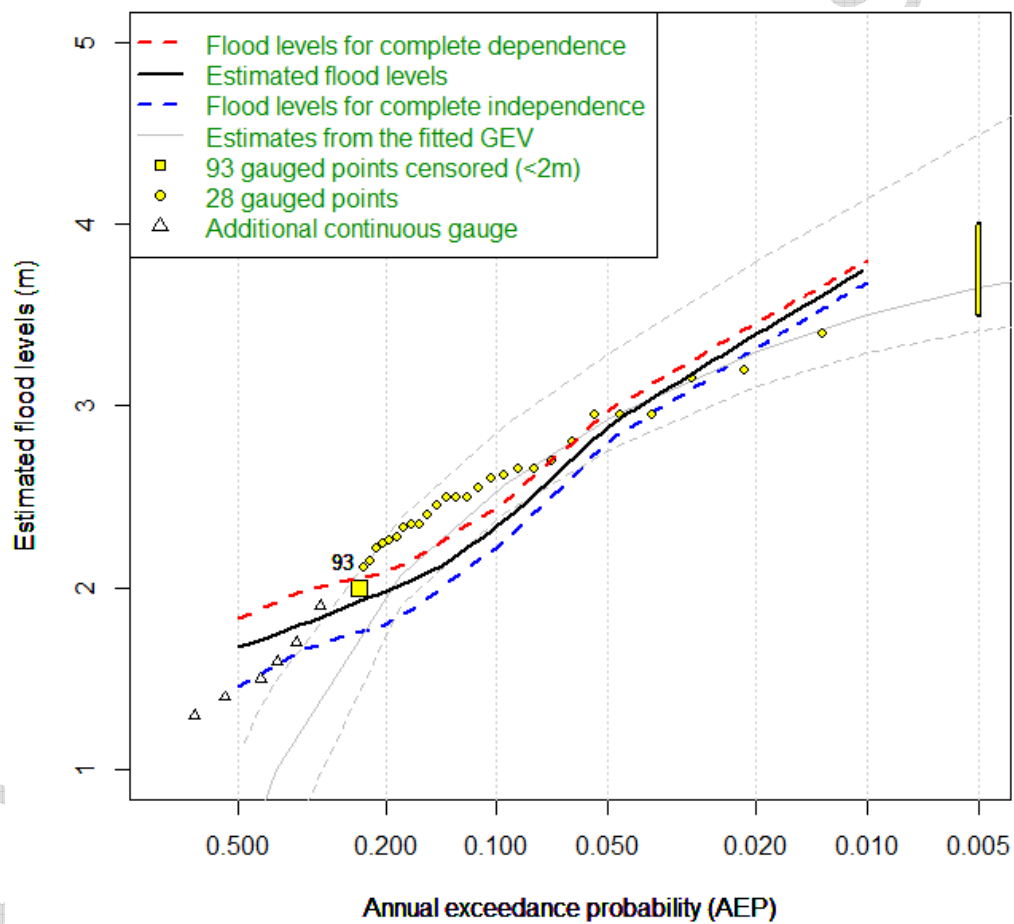


Figure 9.4: Flood levels at Macksville (Pacific Highway Bridge) in the Nambucca river catchment, against the annual exceedance probability (AEP). The dependence parameters with 0 (red dot line) and 1 (blue dot line) represent complete dependence and independence, respectively. The observed flood levels are shown by orange dots. The fitted GEV and its 90% confidence intervals are shown by orange lines.

It is clear from the flood frequency analysis outlined in the preceding paragraph that, based on

the diversity of data sources, it is difficult to obtain a complete understanding of the design flood levels in the Macksville region, so that a comparison between the flood frequency analysis and the joint probability method is not straightforward. The comparison is nonetheless instructive because it provides insight into how the methods are interpreted and should be used to drive further investigation. It is important to use the GEV confidence limits as a backdrop for how the joint probability method is interpreted, and on this basis there is overlap between the two methods for a wide range of AEPs. Nonetheless, in several respects the two methods do not agree as well as might be hoped for and further analysis would be required to establish the reasons. With respect to the GEV distribution, the joint probability results indicated in Figure 9.4, (i) overestimates the lower tail in the AEP range <0.2 , (ii) overestimate in the AEP range $0.2 - 0.05$ and (iii) overestimate the upper tail in the AEP range >0.02 . There are many possible reasons for these discrepancies including

1. Accuracy of the data;
2. Accuracy of methods for attributing AEPs to boundary events (e.g. uncertainty of fitted marginal distributions and translation of rainfall events to flow events);
3. Inadequacy of the hydraulic model for certain ranges of water levels at this location;
4. Assumptions made in the flood frequency analysis (distribution, censoring of data, etc); and
5. Assumptions made in the joint probability method (number of intervals in Table 9.3, appropriateness of logistic model, estimation of alpha parameter based on record length differing from flood study).

Considering these issues for this particular case:

1. The additional points from the continuous gauge in Figure 9.4 suggest that the lower tail region of the frequency distribution may be higher than estimated when using the 121 year record. This issue should be investigated further. It is unclear whether the hydraulic model took these events into account during calibration, which would then have influenced the joint probability method to yield higher estimates than if the 121 year record was used in isolation.
2. This issue is a major reason for the discrepancy and it significantly influences correct interpretation of the joint probability results. Observing the flood frequency estimates, it is clear that there is significant uncertainty due to a single 3-parameter GEV distribution. The joint probability method has two distributions associated with the boundary margins, (the extreme tides distribution and the extreme rainfall distribution) in addition to a dependence parameter and the parameters of the hydraulic model. These are a significant source of uncertainty which is not accounted for in the comparison with the flood frequency analysis (note: the largest source of uncertainty is expected to be the marginal distribution parameters rather than hydraulic model parameters or dependence

parameter). Without computing the uncertainty intervals, it is not possible to formally test the hypothesis that the flood levels from the flood frequency analysis are statistically different to those from the joint probability analysis.

3. Inspecting Table 9.3 for the 2% event with *low astronomical tide* shows a height of 3.32 m which is comparable to the points given in Figure 9.4, the 1964 flood event at 3.2m (2.1% AEP) and the 1950 event at 3.4m (1.3% AEP). For tides greater than the low astronomical tide, the 2% rainfall event gives higher water levels, i.e., the hydraulic model seems to be giving higher water levels than similar observed historical events. Further checking of historic events would better inform this comparison and whether the hydraulic model has good performance for this location and range of events.
4. There are a number of assumptions made in the flood frequency analysis, many of which were illustrated in the preceding paragraphs of this section. Particular concern for further investigation should be given to the skewed shape of the distribution at this location, sensitivity to individual data points, and the model assumptions. One option would be to further investigate regional flood frequency analyses.
5. The joint probability method has a number of assumptions which have been discussed in this report. Attempts to reconcile discrepancies between methods should also take these issues into account. Note that the discrepancies in Figure 9.4 are observed with the independence and complete dependence cases so the issue is more likely to be due to the assumed marginal distributions and the performance of the hydraulic model rather than the joint dependence model (which can only vary between these two extreme cases).

Finally, figure 9.5 shows the flood level estimates of nine different locations in the Nambucca River catchment for AEPs=10% and 1%. These locations are shown in the x axis ordered from downstream to upstream. For AEP=10% the locations from Stuarts Island to Railway Bridge in the middle of the river are more affected by the dependence than other locations. While for the 1% AEP (large flood events), the impact of the dependence is not significant for all locations as the flood levels are dominated by rainfall only (the red dotted line overlaps with the blue dotted line).

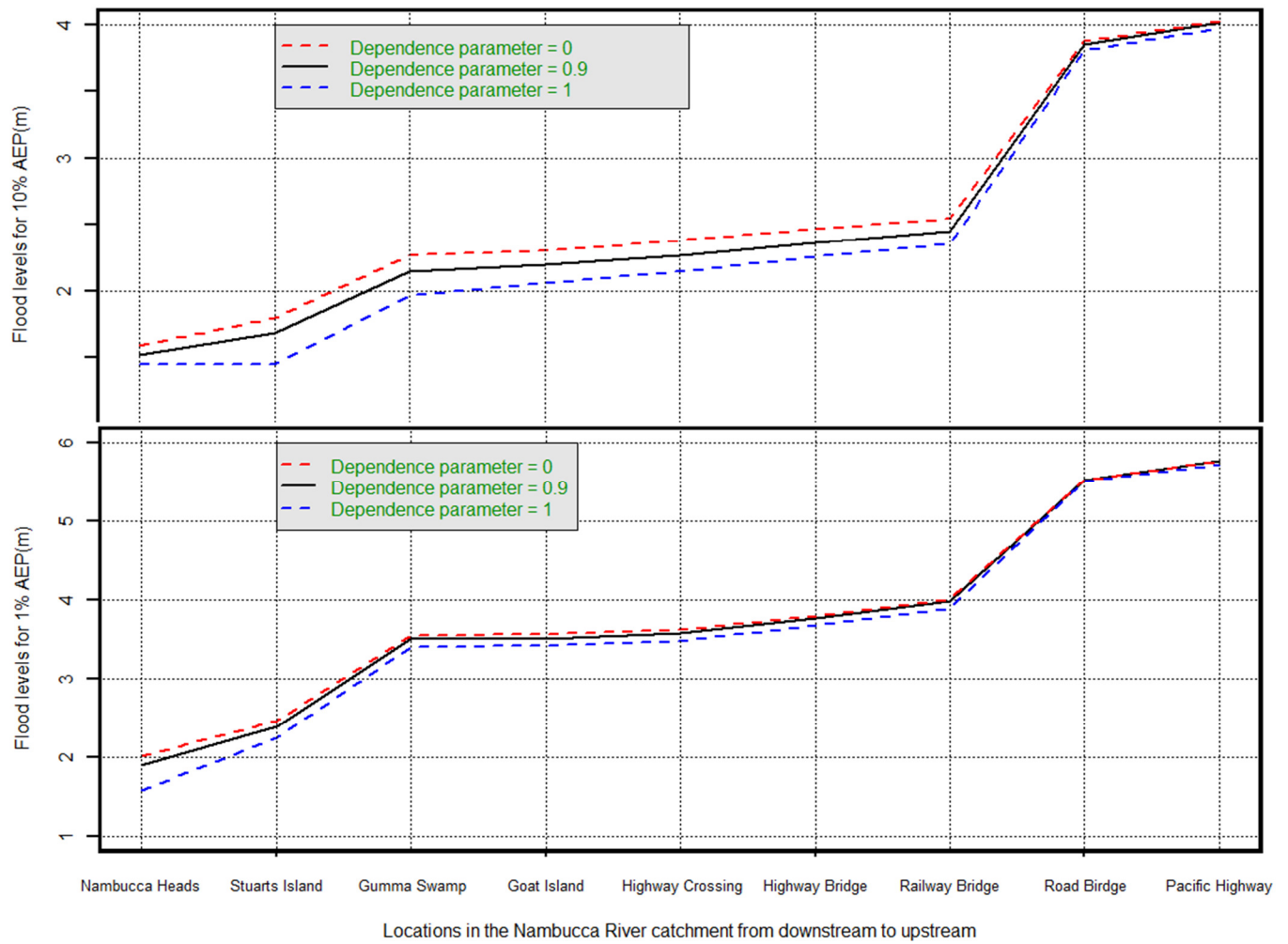


Figure 9.5: Flood levels nine different locations in the Nambucca River catchment for AEPs=10% and 1%. The dependence parameters with 0 (red dot line) and 1 (blue dot line) represent the complete dependence and independence respectively.

Draft

10. Summary and Conclusions

10.1. Development of a map representing dependence strength

This report documents Stage 3 of Project 18 of Australian Rainfall and Runoff Revision. The emphasis of this stage was to investigate the dependence between extreme rainfall and extreme storm surge along the Australian coastline, and to develop a method to incorporate such dependence into estimates of flood risk.

A total of 49 tide gauge locations with long records were used for dependence analysis, together with a further 15 high-quality tide gauges that were taken from the Australian Baseline Sea Level Monitoring Project (ABSLMP) with measuring period from 1991 to 2010. A total of 7,684 good quality daily precipitation stations from across the Australian continent were used to pair with the tide gauges to enable the dependence analysis. In addition, 70 sub-daily gauges were selected for investigating the impact of the storm burst duration and lag between the rainfall and surge event on the dependence strength.

Results show that the majority of the tide gauges along the Australian coastline exhibited statistically significant dependence between extreme rainfall and storm surge. The dependence strength varied as a function to the spatial distance between the rainfall gauge and the tide gauge, the storm burst durations and the lags between the two extreme events (for details see Chapter 6). The detailed results for each tide gauge are given in Appendix D. In addition, an investigation into the asymptotic characteristics of the bivariate extremes (rainfall and surge) showed that the majority of the Australian coastline exhibited asymptotic dependence, so that the rainfall is more likely to co-occur with storm surge when both become increasingly extreme.

To evaluate the influence of storm burst duration, 70 sub-daily rainfall gauges were selected for investigating the influence of the temporal variability (storm burst duration) on the dependence strength along the Australian coastline. The results show that the dependence strength overall increases when the storm burst duration increases from 15 min to 24 hours along the Australian coastline. When longer storm burst durations were considered (>24 hours), some coastal zones exhibited stronger dependence, while others showed approximately constant or slightly weaker dependence relative to 24 hours durations.

In addition to the variation of the storm burst durations, the impact of lags between the extreme rainfall and extreme storm surge was also examined. It was observed that the extreme rainfall is more likely to occur after the extreme storm surge, with lags depending on the storm burst duration and the location, although the dependence between these two processes occurring at the same period is also significant. Given this, the lags may have limited influence on the flood

levels as the peak of the storm surge is not likely to hit the peak of the hydrograph for the catchment, and thus the results were based on zero lag estimates of the dependence parameter.

Based on the analysis, a dependence map is provided (Figure 6.6) to show the spatial variation of the dependence strength along the Australian coastline. A single dependence parameter was used to represent the dependence strength for each region, for three storm burst duration ranges. This map is recommended for use in guidance for practitioners to incorporate the dependence of flood risk analyses along the Australian coastline.

Finally, it is noted that a detailed site-by-site analysis of the dependence behaviour could not identify a consistent regional pattern for the case of complete independence. As a result, the proposed method assumes that all locations may require a joint dependence analysis, but that for some regions the dependence is very weak (0.98).

10.2. A method to translate dependence to estimates of flood risk

A method has been developed to incorporate the dependence between extreme rainfall and extreme storm surge for flood risk analysis. A step by step explanation of this proposed method is given in Chapter 8 and is briefly outline here.

Step 1: A pre-screening analysis to determine whether full joint probability analysis is required.

Step 2: Dependence parameter selection for the location and relevant storm burst duration using Figure 6.6.

Step 3: Flood level modelling using a set of 49 combinations of rainfall and storm tides.

Step 4: Undertake joint probability calculations.

An R package has been developed to estimate the flood levels with a table with flood levels (Table 8.2) and a dependence parameter value selected from the dependence map (Figure 6.6) as inputs.

Two case studies have been presented in this report illustrating the method (i) a drainage system from Perth, Western Australia and (ii) the Nambucca River catchment in New South Wales. These case studies demonstrate the feasibility of the method for arriving at estimates of flood risk based on joint extreme events.

Climate change has not been explicitly accounted for in the development of the proposed method. In particular, the dependence parameters outlined in Figure 6.6 are developed using historical records of rainfall and storm surge, and thus may change as a result of changes in large-scale climate. Based on an assumption that the joint dependence between extreme rainfall

and storm surge remains stationary, the method can be used for a climate change situation by assuming that only the marginal distributions of both the sea level and the rainfall are subject to change. This means climate change projections need to be used for ocean levels (by accounting for sea level rise and possible changes to storm surge height) and extreme rainfall. The climate change-adjusted marginal AEPs are then inserted into Table 8.2 to provide an approximate estimate of the flood level under climate change situations.

10.3. Exclusions and further research

This report describes the first national assessment of the role of dependence between extreme rainfall and storm surge on flood risk along the Australian coastline. The method has been designed to be applicable to a wide range of cases, and relies on the design event-based modelling techniques that are commonly used in flood hydrology practice. As such, some simplifying assumptions were made in developing the techniques, and a number of issues have been reserved for future research. These are outlined below:

- **Uncertainty.** At present, the method focuses on producing ‘best estimates’ of the flood level, and does not provide uncertainty bounds associated with those estimates. Uncertainty can arise from a number of sources, including uncertainty in the marginal probabilities of the rainfall and storm surge, uncertainty in the dependence parameter, uncertainty in the hydrologic and hydraulic model structures used to compute flood levels for different combinations of rainfall and storm surge/tide, and uncertainty in the observational data used to force those models. The uncertainty from all these sources is likely to be significant, and statistical methods (including methods based on Monte Carlo sampling and Bayesian approaches) are increasingly becoming available to enable incorporation of uncertainty into the joint probability models. Research is required on an integrated framework that incorporates all these sources of uncertainty into coastal joint probability problems.
- **Meteorology.** The joint occurrence of rainfall and storm surge usually arises due to common meteorological forcings, such as east coast lows along the eastern coast of Australia, or tropical cyclones along the northern parts of the continent. Typically, such events bring on-shore winds and heavy rainfall, while also contributing an inverse barometric effect that further raises the ocean level. Nevertheless, the investigation described in this report was purely statistical, and did not assess the potential meteorological drivers that cause the joint probability. An improved understanding of the meteorology will potentially lead to an improved understanding of the causes of variations in the dependence parameter along the Australian coastline.
- **Bathymetry.** The storm tide gauges used in this report are sometimes located outside estuaries, and thus will not always accurately represent the lower boundary condition of hydrodynamic models that simulate floods inside estuaries and coastal river systems. The

assumptions of the dependence parameter estimates used in this report are that the *ranking* of storm surge extremes remains consistent between the storm tide gauges and the locations of interest for flood modelling, whereas the *magnitude* need not be. This is because the joint probability method focuses on the probability of extreme rainfall and storm surge occurring on the same day, with the absolute magnitudes of the rainfall and storm surge addressed by the marginal transformations. Nevertheless, factors such as the orientation of the estuary relative to prevailing winds, and other bathymetric effects that influence the magnitude of the storm surge, are likely lead to local variations to the regional dependence parameters given in Figure 6.6. Further research is therefore required on the role of bathymetric and other effects on influencing the dependence between extreme rainfall and storm surge.

- **The relationship between storm surge and storm tide.** The dependence parameters were derived using the combination of rainfall and storm surge, whereas the method is applied to combinations of extreme rainfall and storm tide. An alternative approach is to model the trivariate distribution of extreme rainfall, storm surge and astronomic tide, however this will require more complex joint probability models that account for the distribution of both extreme and non-extreme values of each of the variables. Another approach is to pair the rainfall with storm tide directly, however in this case the focus was on storm surge as it allowed for a better description of the influence of meteorological factors on the dependence, and leaves open the possibility for future research to explore the physical mechanisms that cause the dependence. The assumptions in the method recommended in this report are likely to lead to a slightly upwardly biased estimate of flood risk, as the dependence between extreme rainfall and storm tide is likely to be slightly lower than between extreme rainfall and storm surge.
- **Continuous simulation and dynamic tidal methods.** The methods described in this report assume static tailwater levels, whereas estuaries and other tidal systems are naturally dynamic. To account for dynamic effects, it is likely that it will be necessary to move to a continuous simulation framework, in which riverine levels are estimated continuously over an extended period of time. However such a framework will face a number of challenges, including: (i) the limitations of forcing data, with continuous sub-daily rainfall and storm tide data often not being available at the location of interest; (ii) the difficulty of some models in reproducing extreme events; (iii) challenges associated with stochastically generating continuous series of both rainfall and storm tide to obtain sufficiently long replicates for a detailed flood assessment; and (iv) computational limitations, involved with running fine time-scale hydrodynamic models for potentially hundreds of years.
- **Rarer or more frequent floods.** The method has been tested for AEPs from 50 % to 1 %. Floods more frequent than the 50 % AEP event may be important for applications like water sensitive urban design and environmental flows, but are likely to violate the assumptions of

'extreme' embedded in the extreme value models used in this work, which focus on the tail of the probability distribution. In contrast, the method is theoretically able to produce flood risk estimates for AEPs rarer than the 1 % AEP, but the method has not been tested beyond this magnitude and the uncertainty of the estimates is likely to be very large. The findings of asymptotic dependence described in this report also should be further investigated, to determine whether there are physical constraints on the joint dependence that might be relevant for very rare events.

- **Climate change.** Climate change was not explicitly considered in this work. As discussed in Section 10.2, climate change can be included in the analysis by modifying the marginal distributions of extreme rainfall and extreme storm tide. For example, the modelling outputs in Table 8.2 can be obtained based on assumptions on the future intensity of extreme rainfall and the height of storm tides, corresponding to each of the AEPs. Guidance on how to compute these AEPs is beyond the scope of this report. Furthermore, this method assumes that the dependence parameters given in Figure 6.6 will remain the same in the future, which may not be the case, for example due to a change in the dominant storm-producing mechanisms along the coastline. Therefore, the use of the method described in this report for future climate scenarios should proceed with caution, acknowledging the significant increase in uncertainty associated with such estimates.

Research in the field of coincident extremes is progressing rapidly, with developments in fields ranging from atmospheric physics and meteorology (which helps explain the physical cause of the observed joint dependence), extreme value statistics (which are needed to develop probabilistic estimates of floods that have low exceedance probabilities) and in both inland and coastal flood modelling (Leonard et al, 2014). Further progress in this field is therefore likely to be best served through multidisciplinary research, spanning meteorology, statistics, hydrology and coastal modellers.

The method for flood risk estimation described in this report represents a theoretically valid approach for estimating flood risk in estuarine catchments, however it should be noted that it is unlikely to be the only viable approach, nor will it be the best approach in all circumstances. Methods based on time-stepping continuous simulation models may also be appropriate under some conditions, although at present there is an absence of comparative studies between the method described in this report and those based on continuous simulation, such that it is currently difficult to provide detailed guidance on method selection. Furthermore, where sufficient data is available it may be appropriate to conduct a location-specific assessment of the statistical dependence between extreme rainfall and storm surge/tide, rather than use the dependence parameters provided in Figure 6-6. It is therefore recommended that the ARR guidance describe the method outlined in this report, while simultaneously ensuring that alternative approaches can be used where they can be theoretically justified.

11. References

- Bortot P., Coles S., Tawn J. (2000) The multivariate Gaussian tail model: an application to oceanographic data. *Applied Statistics* 49:31-49.
- Callaghan, J. and P. Helman. 2008. Severe storms on the east coast of Australia 1770-2008. Griffith Centre for Coastal Management, Griffith University, Gold Coast Queensland.
- Coles S.G., Tawn J.A. (1994) Statistical Methods for Multivariate Extremes: An Application to Structural Design. *Journal of the Royal Society. Series C (Applied Statistics)* 43:1-48
- Coles S., Heffernan J., Tawn J. (1999) Dependence measures for extreme value analysis. *Extremes* 2:339-365.
- Coles S.G. (2001) *An Introduction to Statistical Modelling of Extreme Values* Springer, London.
- de Haan, L. (1985), A spectral representation for max-stable processes, *The Annals of Probability*, 12(4), 1194–1204.
- EngTest. (2010) Australian Rainfall and Runoff Revision: Project 18 - Interaction of Coastal Processes and Severe Events - Data Collation Report, Adelaide University, Adelaide. pp. 8.
- Haigh, ID, Wijeratne, EMS, MacPherson, LR, Pattiaratchi, CB, Mason, MS, Crompton, RP, George, S (2012) "Estimating present day extreme water level exceedance probabilities around the coastline of Australia: tides, extra-tropical storm surges and mean sea level" *Climate Dynamics*, DOI 10.1007/s00382-012-1652-1.
- Hawkes P.J., Gouldby B.P., Tawn J.A., Owen M.W. (2002) The joint probability of waves and water levels in coastal engineering design. *Journal of Hydrologic Research* 3:241-251.
- Hunter, J., (2011) "A simple technique for estimating an allowance for uncertain sea-level rise", *Climatic Change*, DOI 10.1007/s10584-011-0332-1.
- Jenkinson, A. F. A., (1955) The frequency distribution of the annual maximum (or minimum) values of meteorological elements, *Quarterly Journal of the Royal Meteorological Society*, 81(348), 158–171. doi:10.1002/qj.49708134804.
- Kotz S., Nadarajah S. (2000) *Extreme Value Distributions: Theory and Applications* Imperial College Press.
- Kuczera (1999) "Comprehensive at-site flood frequency analysis using Monte Carlo Bayesian inference", *Water Resources Research*, 35(5), 1551-1557, DOI: 10.1029/1999WR900012.
- Leonard, M., Westra, S., Phatak, A., Lambert, M., Van Den Hurk, B., McInnes, K., Risbey, J., Schuster, S., Jakob, D., Stafford-Smith, M., (2013). A compound event framework for understanding extreme impacts. *Wiley Interdisciplinary Reviews: Climate Change*, 5, 113-128 Available from: <http://dx.doi.org/10.1002/wcc.252>.
- Lian, J.J., Xu, K., Ma, C., (2013) Joint impact of rainfall and tidal level on flood risk in a coastal city with a complex river network: A case study of fuzhou city, china. *Hydrol. Earth Syst. Sci.*, 17 (2), 679-689
- NSW DECCW. (2009) *Draft Flood Risk Management Guide: Incorporating sea level rise benchmarks in flood risk assessments*, NSW Department of Environment, Climate Change and Water.
- Pickands, J. (1975) Statistical inference using extreme order statistics, *Annals of Statistics*, 3, 119-131.
- Pugh D.T. (1987) *Tides, Surges, and Mean Sea-Level*, Chichester.
- Resnick, S.I. (1987), *Extreme values, regular variation, and point processes*, Berlin Heidelberg New York: Springer.
- Svensson C., Jones D.A. (2002) Dependence between extreme sea surge, river flow and precipitation in east Britain. *International Journal of Climatology* 22:1149-1168.
- Svensson C., Jones D.A. (2004) Dependence between sea surge, river flow and precipitation in south and west Britain. *Hydrological Earth Systems Science* 8:973-992.
- Svensson C., Jones D.A. (2006) *Joint Probability: Dependence between extreme sea surge, river flow and precipitation: A study in South and West Britain*. R&D Technical Report FD2308/TR3, DEFRA.
- SREX (2012). *Managing the Risks of Extreme Events and Disasters to Advance Climate Change Adaptation*. A Special Report of Working Groups I and II of the Intergovernmental Panel on Climate Change, (Field C.B, Barros V, Stocker T.F, Qin D, Dokken D.J, Ebi K.L, Mastrandrea

- M.D, Mach K.J, Plattner GK, Allen S.K. et al. (eds.)). Cambridge University Press, Cambridge, UK, and New York, NY, USA, 582 pp.
- Tawn J. (1988) Bivariate extreme value theory: Models and Estimation. *Biometrika* 75:397-415.
- Westra, S., (2012), Australian Rainfall and Runoff Revision Project 18: Interaction of Coastal Processes and Severe Weather Events: Phase 1 – Pilot Study into Joint Probability Modelling of Extreme Rainfall and Storm Surge in the Coastal Zone, available online from: http://www.arr.org.au/Website_links/ARR_Project18_Stage2_Report_Final.pdf.
- WMAwater, (2011). Review of Bellinger, Kalang and Nambucca River Catchment Hydrology.
- WMAwater, (2013). Hydraulic Modelling Report Nambucca River and Warrell Creek.
- White, C.J., (2009). The use of joint probability analysis to predict flood frequency in estuaries and tidal rivers. PhD Thesis, School of Civil Engineering and the Environment, University of Southampton.
- Zheng, F., Westra, S., Sisson, S.A., (2013a). Quantifying the dependence between extreme rainfall and storm surge in the coastal zone. *Journal of Hydrology*, 505 (0), 172-187.
- Zheng, F., Westra S. Sisson S., Leonard M. (2013b). Modelling the dependence between extreme rainfall and storm surge to estimate coastal flood risk, *Water Resources Research*, submitted.
- Zheng, F. Leonard M. and Westra S. (2013c). An efficient bivariate integration method for estimating flood risk, *Water Resources Research*, in preparation.
- Zheng, F. Leonard M. and Westra S. (2013d). Addressing the issues and the practical methods about joint dependence modelling for coastal flood risk estimation, *Hydrology and Earth System Sciences*, in preparation.
- Zheng, F., Westra S., Sisson S., Leonard M. (2013e). Flood risk estimation in Australia's coastal zone: modelling the dependence between extreme rainfall and storm surge, 35th Hydrology and Water Resources Symposium, 24 – 27 February 2014, Perth, Australia.

Appendix A – Information on the sub-daily rainfall gauges

Table A1: Sub-daily rainfall gauges (70)

Sub-daily station rainfall ID	Latitude	Longitude	Record length (years)	Sub-daily station rainfall ID	Latitude	Longitude	Record length (years)
plv002014	-15.6547	128.7092	28	plv031011	-16.8736	145.7458	60
plv003003	-17.9475	122.2353	55	plv031066	-16.995	145.4253	44
plv004032	-20.3725	118.6317	52	plv031083	-17.84	145.5956	39
plv004035	-20.7767	117.1456	31	plv032040	-19.2483	146.7661	50
plv005061	-20.7278	116.7483	24	plv032042	-17.9364	145.9256	31
plv005069	-21.6392	116.3308	27	plv032063	-19.1647	145.4208	37
plv006011	-24.8878	113.67	43	plv033013	-20.5534	147.8464	30
plv006022	-25.0544	115.21	18	plv033087	-21.5286	149.0006	38
plv008051	-28.7953	114.6975	48	plv033119	-21.1172	149.2169	43
plv008138	-30.8408	116.7267	38	plv035025	-23.6455	149.3308	41
plv008267	-28.3517	114.5778	14	plv039006	-24.3789	150.5164	49
plv009034	-31.9556	115.8697	43	plv039083	-23.3753	150.4775	63
plv009510	-33.9575	116.1375	38	plv040126	-25.5161	152.7156	38
plv009592	-34.4478	116.0433	28	plv040214	-27.4778	153.0306	79
plv009631	-33.6031	121.7828	25	plv040223	-27.4178	153.1142	48
plv009741	-34.9414	117.8022	35	plv040282	-26.6431	152.9392	46
plv009789	-33.83	121.8925	32	plv061078	-32.7932	151.8359	48
plv010622	-33.9644	118.4889	33	plv061089	-32.0632	150.9272	45
plv014015	-12.4239	130.8925	47	plv061238	-32.8143	151.3025	42
plv014508	-12.2741	136.8203	13	plv066062	-33.8607	151.205	86
plv014908	-13.6817	130.6367	12	plv066062	-33.8607	151.205	86
plv014938	-13.7379	130.6834	23	plv070014	-35.3049	149.2014	55
plv018012	-32.1297	133.6976	37	plv079052	-37.2297	141.9608	42
plv018052	-32.8361	135.15	23	plv081013	-36.3717	145.7048	49
plv018116	-33.7081	136.5026	32	plv085072	-38.1156	147.1322	48
plv018139	-33.5085	135.2928	36	plv086071	-37.8075	144.97	100
plv021060	-33.2025	138.6024	47	plv086142	-37.572	145.5014	45
plv022801	-35.7529	136.5938	31	plv088023	-37.2313	145.9124	43
plv023000	-34.9254	138.5869	71	plv090087	-38.6636	143.4495	37
plv023034	-34.9524	138.5204	37	plv091009	-41.0661	145.9431	35
plv023763	-34.7122	138.9469	30	plv091104	-41.5397	147.2033	62
plv023801	-34.9482	138.8071	33	plv094008	-42.8339	147.5033	44
plv026021	-37.7473	140.7739	54	plv094029	-42.8897	147.3278	86
plv027006	-13.7642	143.1178	28	plv097008	-42.0661	145.5681	34
plv027042	-12.6267	141.8836	29	plv031012	-16.8736	145.7458	60

Appendix B – Procedures for obtaining the dependence parameter

The fitting procedures for the threshold-excess model

The fitting procedures of the bivariate threshold-excess and point process models are briefly discussed here, with details of both methods given in Zheng *et al.* (2013b). Typically, the following three steps are involved in fitting the bivariate threshold-excess model:

Step 1: *Determine valid thresholds, u , for both margins, above which the data can be viewed as ‘extreme’ for the purpose of fitting the GPD given in Equation (5.2).* The selection of u represents a trade-off between bias and variance for the parameter estimation. A threshold that is too low produces a precise estimate due to large amount of data available, but will be biased as the asymptotic justification of the extreme value model will not be valid even as an approximation. Conversely, if the threshold is too high, the extreme value model will likely provide a reasonable approximation to the data, but the limited sample size will result in highly variable parameter estimates. Coles (2001) proposed a method that was based on an assessment of mean residual life plots and plots of the scale and shape parameter as a function of the threshold to determine the valid threshold values. More details on threshold selection for the extreme rainfall and storm surge dataset are given in Zheng *et al.* (2013a).

Step 2: *Fit margins above the thresholds using the GPD and then transform margin values to standard Fréchet distributions.* The parameters were estimated using the maximum likelihood method. The data (x,y) above the thresholds were transformed to follow standard Fréchet distributions, (\tilde{x}, \tilde{y}) , by substituting the estimated Pareto parameters $\hat{\sigma}$ and $\hat{\xi}$ into the following equation:

$$\tilde{z} = -(\log\{1 - \zeta[1 + \frac{\hat{\xi}(z-u)}{\hat{\sigma}}]^{-1/\hat{\xi}}\})^{-1} \quad (\text{B1})$$

where $\zeta = \Pr\{Z > u\}$ and u is an appropriately high threshold. After transforming both margins $(X, Y) \rightarrow (\tilde{X}, \tilde{Y})$, we can model the transformed extremes via:

$$G(x, y) = \exp\{-V(\tilde{x}, \tilde{y})\} \quad x > u_x, y > u_y \quad (\text{B2})$$

for sufficiently high thresholds u_x and u_y , where \tilde{x} and \tilde{y} are standard Fréchet-transformed values of x and y respectively.

Step 3: *Specify and fit a parametric family distribution model (the logistic model was used in this study).* The data (\tilde{x}, \tilde{y}) with either margin exceeding their corresponding threshold can be

used to estimate the dependence parameter α in the logistic model (Equation (5.4)) via the censored likelihood approach (for details of the censored likelihood method see Coles and Tawn (1991)).

The fitting procedures of point process model

de Haan (1985) described the point process method in terms of radial components $r = x + y$ and angular components $w = x / r$, with the intensity function of N given as:

$$\lambda(dr \times dw) = 2 \frac{dr}{r^2} dH(w) \quad (\text{B3})$$

where $h(w)=dH(w)$ when the density function exists. The function $G(x,y)$ corresponding to $h(w)$ also conforms to the constraints of the family of bivariate extreme value distributions (Coles 2001). The fitting procedures of the point process model are given below.

Step 1. Marginal threshold selection and transformation. The marginal threshold selection method is the same as for the threshold-excess method. The Pareto parameter estimates are then used to transform the full margins to the standard Fréchet distributions through the transformation proposed by Coles and Tawn (1994):

$$\tilde{z}_i = \Psi(z_i) = \begin{cases} - \left(\log \left\{ 1 - F(u) \left[1 + \frac{\hat{\xi}(z-u)}{\hat{\sigma}} \right]^{-1/\hat{\xi}} \right\} \right)^{-1} & z_i > u \\ - \{ \log F(z_i) \}^{-1} & z_i \leq u \end{cases} \quad (\text{B4})$$

where $z=x$ and $z=y$; $\hat{\sigma}$ and $\hat{\xi}$ are the estimated Pareto parameters, and $F(z_i)$ is the empirical distribution function, estimated by $F(z_i) = i/(n+1)$, where i is the observation rank and n is the total number of data points.

Step 2: Joint threshold (r_0) selection. The intensity function given in Equation (B3) is only valid for (w,r) with r above a suitable threshold r_0 , and where the angular component w is independent of the radial component r . Given this constraint, Coles and Tawn [1994] suggested a method for determining the threshold r_0 by examining the empirical histograms of $\{w \mid r > r_0\}$ for a range of possible r_0 values, and then identifying r_0 as the smallest value above which the shape of the histogram is apparently stable. For details on how to select the threshold r_0 for the rainfall-surge dataset, see Zheng *et al.* (2013b).

Step 3: Fitting the parametric model $h(w)$. Having determined r_0 , a likelihood function can be

constructed for those values of $w \mid r > r_0$ which are drawn from the spectral density function $h(w)$ under the point process method. This leads to the estimate of the dependence parameter α for the logistic model with $h(w)$ given in Equation (5.5).

Draft for discussion

Appendix C – Selecting the statistical model

Performance comparison between threshold-excess and point process models

Zheng *et al.* (2013b) conducted a systematic analysis on the performance of the threshold-excess and point process methods. In their study, synthetic datasets were generating using the bivariate logistic model as shown in Equation (5.4) with various dependences ranging from $\alpha=0.5$ to $\alpha=0.99$. For each α , 1000 replicate datasets were generated, each comprising 10,000 data points. Then the threshold-excess logistic model and point process logistic model were employed to estimate the dependence parameter $\hat{\alpha}$ for these synthetic datasets to enable a comparison with the true parameter α . The fitting procedures are shown in Section 4.3 for both methods. In that study, the following conclusions were made:

- (1) The threshold-excess method produces unbiased dependence parameter estimates. However, its practical application may be limited because it does not fully model situations where only one of the two variables is extreme.
- (2) The point process is able to model the full distribution of extremes. However, it produce overestimates of the dependence strength in the observed data, with the bias particularly significant in the case of weak extremal dependence ($\alpha > 0.7$). In addition, the bias was found to be independent of sample sizes.
- (3) The estimates using the threshold-excess model exhibited a larger variance than those using the point process model.

Figure C1 gives the mean (solid lines) and 95% confidence interval (dashed lines) of the parameter estimates ($\hat{\alpha}$) against the true value (α). The threshold-excess method (grey lines) consistently produces unbiased parameter estimates regardless of the level of dependence (the $y=x$ line is displayed in thick black). For the point process method, we used three radial thresholds: $r_0 = \exp(4)/n$ (the red line with circles), $r_0 = \exp(4.5)/n$ (the blue line with squares), and $r_0 = \exp(5)/n$ (the green line with triangles), where n is the number of data points. For each threshold, there is a clear bias in the estimates of α , with the magnitude of the bias becoming larger as α increases (i.e. greater bias for weaker dependence). The bias, which leads to an overestimate of the dependence strength, also increases as the radial threshold decreases. It was observed that the variance of the parameter estimate obtained using the threshold-excess model is larger than that from the point process model as shown in Figure C1 by the width of the confidence intervals.

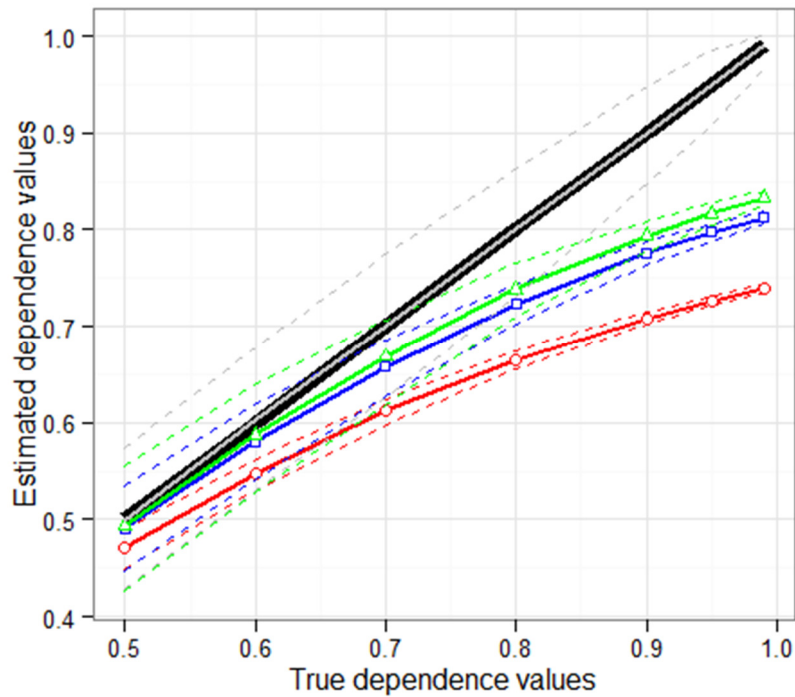


Figure C1. Parameter estimates (solid lines) for the threshold method (the grey line) and point process method with threshold $r_0 = \exp(4)/n$ (the red line with circles), $\exp(4.5)/n$ (the blue line with squares) and $\exp(5)/n$ (the green line with triangles), where n is the number of data points. 95% confidence intervals are given as dashed lines with the same colour as the estimates for each method. The thick black line indicates the $y=x$ line.

The reason behind the differences in parameter estimates is that the point process method makes different usage of the observed data compared to the threshold-excess method. The former assumes the validity of the point process limit in the entire region bounded by the radial threshold and two axes (see right panel of Figure 5.1), and makes full use of the dependence observed between X and Y in this region. In contrast, the threshold-excess model assumes the accuracy of the limiting model only in the joint upper quadrant, and makes use of the margins of the joint observations (X, Y) in the regions when only one variable is extreme (see left panel of Figure 5.1). The implications are: (i) the point process model takes the events with only one component being extreme as joint extremes, in addition to the events with extreme levels at both components, resulting in an overestimation of dependence strength particularly for datasets with weak dependence; and (ii) the point process method typically will use more data points for parameter estimation than the threshold-excess method, producing a smaller estimation variance.

Selection of model to be used in this study

To investigate the implications of the parameter estimates of the two methods (threshold-excess and point process methods) to the resultant flood risk, a study was undertaken to compare the number of extreme events obtained using the two methods with the estimated $\hat{\alpha}$ and that from

the observed datasets for various extreme regions. In this study, all extremes defined using the point process method (events above the yellow curve r_0) were divided into five different regions based on the values of the angular component (w) as shown in the top left panel of Figure C2. These include regions with $w=(0, 0.2]$, $w=(0.2, 0.4]$, $w=(0.4, 0.6]$, $w=(0.6, 0.8]$, and $w=(0.8, 1.0]$. The events in the region with $w=(0.4, 0.6]$ represent the jointly occurring extremes as two components of these events are similar in terms of the magnitude (w is approximately 0.5), while events in the regions with $w=(0, 0.2]$ and $w=(0.8, 1.0]$ represent the situation where only one component is extreme.

A total of 1000 observed datasets with daily rainfall paired with daily maximum storm surge were used for the analysis. For each dataset, the threshold for the point process method was selected to be $\exp(4.5)/n$. The number of observed events for every 10,000 data points located at various extreme regions (different w ranges) were recorded. Then the threshold-excess and point process logistic models were respectively employed to estimate the α for the dataset. Finally, 100 synthetic datasets were generated using the $\hat{\alpha}$ obtained from each method (the number of data points in each synthetic dataset was the same as the corresponding observed dataset) and the number of events for every 10,000 data points located at each extreme region were estimated by taking the average of the 100 synthetic datasets. The red and blue circles in Figure C2 were the result of the observed number of events versus the number of events estimated from the fitted threshold-excess and point process methods respectively.

It can be observed that the estimates from the fitted point process method (blue circles) are significantly higher than those from the observed datasets for extreme regions with $w=(0.2, 0.4]$, $w=(0.4, 0.6]$, and $w=(0.6, 0.8]$. For example, when the number of observed events located in $w=(0.4, 0.6]$ was 5, the number of events in such as region estimated from the point process method was approximately 18 as can be seen from Figure C2. This suggests that the point process method appreciably overestimate the number of jointly occurring events and hence overestimate the dependence, resulting in a severe overestimation of the flood risk ultimately.

The number of events in the regions with $w=(0, 0.2]$ and $w=(0.8, 1.0]$ was underestimated as shown in Figure C2 when using the fitted point process model. This is expected since the number of points in the other three extreme regions was overestimated given that the total number of events above the threshold $r_0 = \exp(4.5)/n$ was approximately fixed.

In extreme regions with $w=(0, 0.2]$ and $w=(0.8, 1.0]$, the estimates produced by the threshold-excess model match well with the number of observed events. This observation can also be approximately made for extreme regions with $w=(0.2, 0.4]$, $w=(0.4, 0.6]$, and $w=(0.6, 0.8]$ in terms of the trend lines (red lines in Figure C2), although the variance of the estimates was significant in these extreme regions.

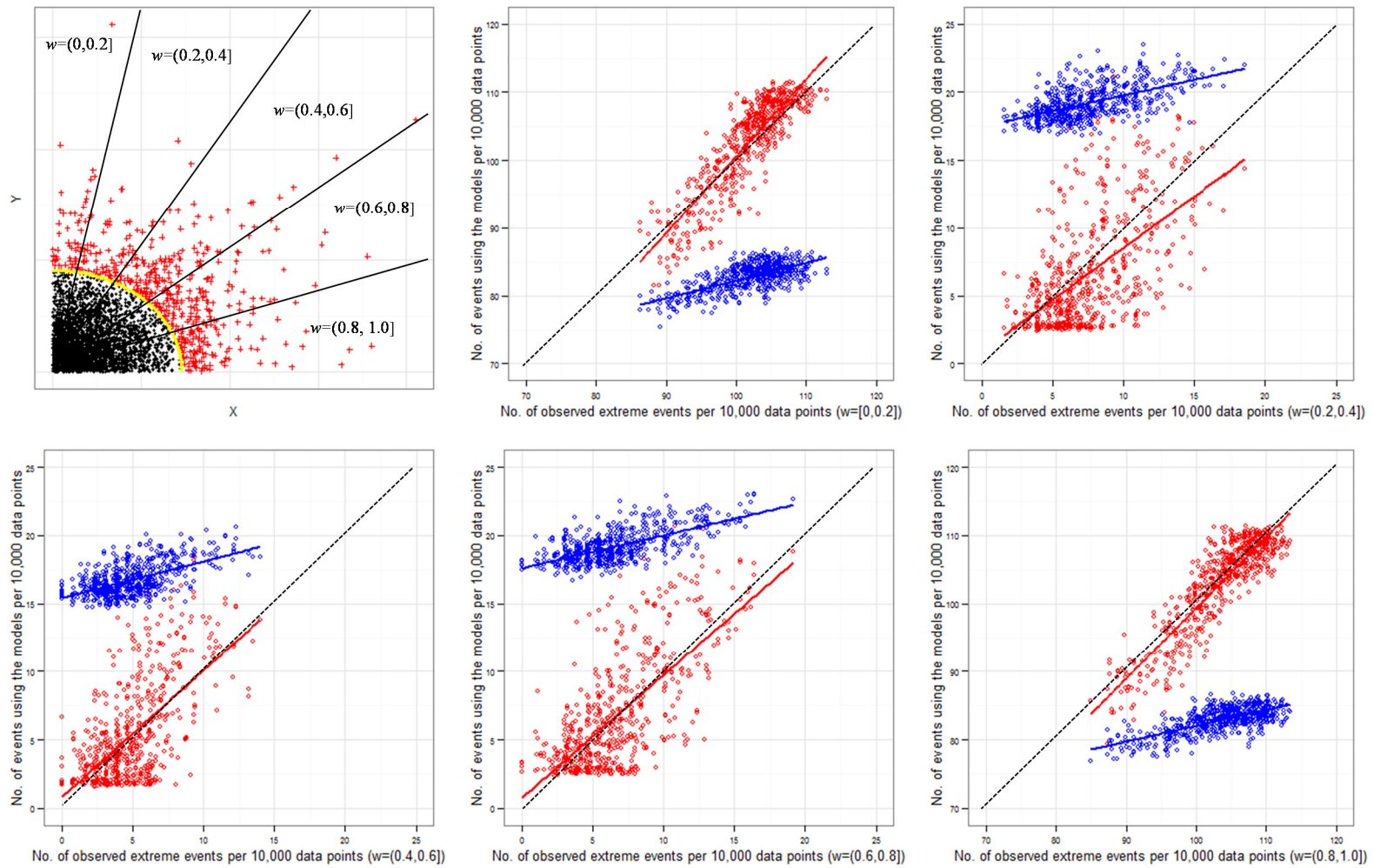


Figure C2. The number of observed extreme events versus the number of extreme events obtained using the fitted threshold-excess (red circles) and points process (blue circles) models for various extreme regions including $w=(0, 0.2]$, $w=(0.2, 0.4]$, $w=(0.4, 0.6]$, $w=(0.6, 0.8]$, and $w=(0.8, 1.0]$. The red and blue lines represent linear trends for the fitted threshold-excess and points process models. The black dot line indicates the $y=x$ line.

Based on the findings in this study and the observations made in Zheng *et al.* (2013b), the following conclusions can be made:

- (1) The threshold-excess model is able to correctly quantify the dependence strength, although the simulation is only based on the joint extreme events in the upper quadrant with all components greater than their corresponding thresholds. In terms of the flood risk estimation, in addition to the jointly occurring extreme events, events with only one extreme component (such as an extreme rainfall event with no surge or an extreme storm surge event with no rainfall) can also cause floods in the coastal catchments. This implies that incorporating events with single extreme components ($w=(0, 0.2]$ and $w=(0.8, 1.0]$) into modelling is very important to correctly estimate the flood risk. Given this, the practical application of the threshold-excess model may be limited.
- (2) In contrast to the threshold-excess model, the point process method is able to handle all extreme regions since all events with their radial components greater than a suitably high threshold (r_0) are modelled. However, the point process method was found to produce severe bias (overestimate) in dependence strength particularly for datasets with weak dependence strength, for details see Zheng *et al.* (2013b). The dependence between extreme rainfall and extreme storm surge along the Australian coastline was detected to be statistically significant but weak, with $\hat{\alpha}$ between 0.9 and 0.95 for the majority of the tide gauges (details for this see Chapter 6). For such weak dependence, the use of the point process method will produce a severe overestimation of the resultant flood risk along the Australian coastline.
- (3) Based on the results given in Figure C2, the point process method with $\hat{\alpha}$ using the threshold-excess model was found to match reasonably well with the observed datasets in terms of the number of extreme events in different regions. In this study, to minimise the impact of sample variability as shown in regions with $w=(0.2, 0.4]$, $w=(0.4, 0.6]$, and $w=(0.6, 0.8]$ in Figure C2, the value of the dependence parameter α for each tide gauge was obtained by taking the mean of α for all the rainfall gauges with a distance less than 30 km from a tide gauge (for details see Chapter 6). This distance was selected as it is likely to encompass the set of rain gauges that are located in the catchments near the tide gauge.

Based on above analysis, we decided to use the point process model but with parameter estimates from the threshold-excess model to incorporate the dependence into flood risk analysis along the Australian coastline. This resulted in more uncertain estimates of the dependence parameter (due to the higher variance of the threshold-excess model) at a single location, tide-gauge and rain-gauge pair, and duration, but this was considered preferable to the significant bias of the point process approach. Furthermore, the dependence map in Figure 6.6

involved multiple levels of averaging: (i) multiple rain gauges were paired with each tide gauge, and the average of all the dependence values within a 30 km radius of the tide gauge was taken; (ii) each region involves averaging the dependence value at multiple tide gauges; and (iii) each duration interval involves averaging the dependence value across multiple durations. This averaging is likely to significantly reduce the dependence parameter variance, and thus lead to more accurate estimates of joint dependence.

Draft for discussion

Appendix D –The detailed results for each tide gauge

Draft for discussion